

Geometrical properties of local dynamics in Hamiltonian systems: the Generalized Alignment Index (GALI) method

Ch. Skokos^{a,b,*}, T.C. Bountis^a, Ch. Antonopoulos^a

^a*Department of Mathematics, Division of Applied Analysis and Center for Research and Applications of Nonlinear Systems (CRANS), University of Patras, GR-26500 Patras, Greece*

^b*Astronomie et Systèmes Dynamiques, IMCCE, Observatoire de Paris, 77 avenue Denfert-Rochereau, F-75014, Paris, France*

Abstract

We investigate the detailed dynamics of multidimensional Hamiltonian systems by studying the evolution of volume elements formed by unit deviation vectors about their orbits. The behavior of these volumes is strongly influenced by the regular or chaotic nature of the motion, the number of deviation vectors, their linear (in)dependence and the spectrum of Lyapunov exponents. The different time evolution of these volumes can be used to identify rapidly and efficiently the nature of the dynamics, leading to the introduction of quantities that clearly distinguish between chaotic behavior and quasiperiodic motion on N -dimensional tori. More specifically we introduce the Generalized Alignment Index of order k (GALI_k) as the volume of a generalized parallelepiped, whose edges are k initially linearly independent unit deviation vectors from the studied orbit whose magnitude is normalized to unity at every time step. We show analytically and verify numerically on particular examples of N degree of freedom Hamiltonian systems that, for chaotic orbits, GALI_k tends exponentially to zero with exponents that involve the values of several Lyapunov exponents. In the case of regular orbits, GALI_k fluctuates around non-zero values for $2 \leq k \leq N$ and goes to zero for $N < k \leq 2N$ following power laws that depend on the dimension of the torus and the number m of deviation vectors initially tangent to the torus: $\propto t^{-2(k-N)+m}$ if $0 \leq m < k - N$, and $\propto t^{-(k-N)}$ if $m \geq k - N$. The GALI_k is a generalization of the Smaller Alignment Index (SALI) ($\text{GALI}_2 \propto \text{SALI}$). However, GALI_k provides significantly more detailed information on the local dynamics, allows for a faster and clearer distinction between order and chaos than SALI and works even in cases where the SALI method is inconclusive.

Key words: Hamiltonian systems, Chaos detection methods, Chaotic motion

PACS: 05.45.-a, 05.45.Jn, 05.45.Ac

1 Introduction

Determining the chaotic or regular nature of orbits in *conservative* dynamical systems is a fundamental issue of nonlinear science. The difficulty with conservative systems, of course, is that regular and chaotic orbits are distributed throughout phase space in very complicated ways, in contrast with dissipative systems, where all orbits eventually fall on regular or chaotic attractors. Over the years, several methods distinguishing regular from chaotic motion in conservative systems have been proposed and applied, with varying degrees of success. These methods can be divided in two major categories: Some are based on the study of the evolution of small deviation vectors from a given orbit, while others rely on the analysis of the particular orbit itself.

The most commonly employed method for distinguishing between order and chaos, which belongs to the category related to the study of deviation vectors, is the evaluation of the maximal Lyapunov Characteristic Exponent (LCE) σ_1 ; if $\sigma_1 > 0$ the orbit is chaotic. The theory of Lyapunov exponents was applied to characterize chaotic orbits by Oseledec [1], while the connection between Lyapunov exponents and exponential divergence of nearby orbits was given in [2,3]. Benettin et al. [4] studied the problem of the computation of all LCEs theoretically and proposed in [5] an algorithm for their numerical computation. In particular, σ_1 is computed as the limit for $t \rightarrow \infty$ of the quantity

$$L_1(t) = \frac{1}{t} \ln \frac{\|\vec{w}(t)\|}{\|\vec{w}(0)\|}, \text{ i.e. } \sigma_1 = \lim_{t \rightarrow \infty} L_1(t), \quad (1)$$

where $\vec{w}(0)$, $\vec{w}(t)$ are deviation vectors from a given orbit, at times $t = 0$ and $t > 0$ respectively. It has been shown that the above limit is finite, independent of the choice of the metric for the phase space and converges to σ_1 for almost all initial vectors $\vec{w}(0)$ [1,4,5]. Similarly, all other LCEs, σ_2 , σ_3 etc. are computed as the limits for $t \rightarrow \infty$ of some appropriate quantities, $L_2(t)$, $L_3(t)$ etc. (see [5] for more details). We note that throughout the present paper, whenever we need to compute the values of the maximal LCE or of several LCEs we apply respectively the algorithms proposed by Benettin et al. [2,5]. Since 1980, new methods have been introduced for the effective computation of LCEs (e. g. [6], see also [7] and references therein). The true power of these techniques is revealed in the study of multi-dimensional systems, when only a small

* Corresponding author.

Email addresses: hskokos@imcce.fr (Ch. Skokos), bountis@math.upatras.gr (T.C. Bountis), antonop@math.upatras.gr (Ch. Antonopoulos).

URLs: <http://www.imcce.fr/~hskokos> (Ch. Skokos),
<http://www.math.upatras.gr/~bountis> (T.C. Bountis),
<http://www.math.upatras.gr/~antonop> (Ch. Antonopoulos).

number of LCE are of interest. In such cases, these methods are significantly more efficient than the method of [5], which computes the whole spectrum of LCEs. On the other hand, they are less or equally efficient when compared with the method of [2] for the computation of the maximal LCE, whose value is sufficient for the determination of the regular or chaotic nature of an orbit.

Among other chaoticity detectors, belonging to the same category with the evaluation of the maximal LCE, are the fast Lyapunov indicator (FLI) and its variants [8,9,10,11,12], the mean exponential growth of nearby orbits (MEGNO) [13,14], the smaller alignment index (SALI) [15,16,17], the relative Lyapunov indicator (RLI) [18], as well as methods based on the study of power spectra of deviation vectors [19], as well as spectra of quantities related to these vectors [20,21,22]. In the category of methods based on the analysis of a time series constructed by the coordinates of the orbit under study, one may list the frequency map analysis of Laskar [23,24,25,26,27,28], the method of the low frequency power (LFP) [29,30], the ‘0–1’ test [31], as well as some other more recently introduced techniques [32,33].

In the present paper, we generalize and improve considerably the SALI method mentioned above by introducing the Generalized ALignment Index (GALI). This index retains the advantages of the SALI – i.e. its simplicity and efficiency in distinguishing between regular and chaotic motion – but, in addition, is faster than the SALI, displays power law decays that depend on torus dimensionality and can also be applied successfully to cases where the SALI is inconclusive, like in the case of chaotic orbits whose two largest Lyapunov exponents are equal or almost equal.

For the computation of the GALI we use information from the evolution of *more than two* deviation vectors from the reference orbit, while SALI’s computation requires the evolution of only two such vectors. In particular, GALI_k is proportional to ‘volume’ elements formed by k initially linearly independent unit deviation vectors whose magnitude is normalized to unity at every time step. If the orbit is chaotic, GALI_k goes to zero exponentially fast by the law

$$\text{GALI}_k(t) \propto e^{-[(\sigma_1 - \sigma_2) + (\sigma_1 - \sigma_3) + \dots + (\sigma_1 - \sigma_k)]t}. \quad (2)$$

If, on the other hand, the orbit lies in an N -dimensional torus, GALI_k displays the following behaviors: Either

$$\text{GALI}_k(t) \approx \text{constant for } 2 \leq k \leq N, \quad (3)$$

or, if $N < k \leq 2N$, it decays with *different power laws*, depending on the number m of deviation vectors which initially lie in the tangent space of the

torus, i. e. :

$$\text{GALI}_k(t) \propto \begin{cases} \frac{1}{t^{2(k-N)-m}} & \text{if } N < k \leq 2N \text{ and } 0 \leq m < k - N \\ \frac{1}{t^{k-N}} & \text{if } N < k \leq 2N \text{ and } m \geq k - N \end{cases} \quad (4)$$

So, the GALI allows us to study more efficiently the *geometrical* properties of the dynamics in the neighborhood of an orbit, especially in higher dimensions, where it allows for a much faster determination of its chaotic nature, overcoming the limitations of the SALI method. In the case of regular motion, GALI_k is either a constant, or decays by power laws that depend on the dimensionality of the subspace in which the orbit lies, which can prove useful e.g., if our orbits are in a ‘sticky’ region, or if our system happens to possess fewer or more than N independent integrals of the motion (i.e. is partially integrable or super-integrable respectively).

This paper is organized as follows: In section 2, we recall the definition of the SALI describing also its behavior for regular and chaotic orbits of Hamiltonian flows and symplectic maps. In section 3, we introduce the GALI_k for k deviation vectors, explaining in detail its numerical computation, while in section 4 we study theoretically the behavior of the new index for chaotic and regular orbits. Section 5 presents applications of the GALI_k approach to various Hamiltonian systems of different numbers of degrees of freedom, concentrating on its particular advantages. Finally, in section 6, we summarize the results and present our conclusions, while the appendices are devoted respectively to the definition of the wedge product and the explanation of the explicit connection between GALI_2 and SALI.

2 The SALI

The SALI method was introduced in [15] and has been applied successfully to detect regular and chaotic motion in Hamiltonian flows as well as symplectic maps [34,16,35,36,17,37,38,39,40,41,42,43,44]. It is an index that tends exponentially to zero in the case of chaotic orbits, while it fluctuates around non-zero values for regular trajectories of Hamiltonian systems and $2N$ -dimensional symplectic maps with $N > 1$. In the case of 2-dimensional (2D) maps, the SALI tends to zero both for regular and chaotic orbits but with very different time rates, which allows us again to distinguish between the two cases [15]: In particular the SALI tends to zero following an exponential law for chaotic orbits and decays to zero following a power law for regular orbits.

The basic idea behind the success of the SALI method (which essentially distinguishes it from the computation of LCEs) is the introduction of one

additional deviation vector with respect to a reference orbit. Indeed, by considering the relation between two deviation vectors (instead of one deviation vector and the reference orbit), one is able to circumvent the difficulty of the slow convergence of Lyapunov exponents to non-zero (or zero) values as $t \rightarrow \infty$.

In order to compute the SALI, therefore, one follows simultaneously the time evolution of a reference orbit along with two deviation vectors with initial conditions $\vec{w}_1(0)$, $\vec{w}_2(0)$. Since we are only interested in the directions of these two vectors we normalize them, at every time step, keeping their norm equal to 1, setting

$$\hat{w}_i(t) = \frac{\vec{w}_i(t)}{\|\vec{w}_i(t)\|}, \quad i = 1, 2 \quad (5)$$

where $\|\cdot\|$ denotes the Euclidean norm and the hat ($\hat{\cdot}$) over a vector denotes that it is of unit magnitude. The SALI is then defined as:

$$\text{SALI}(t) = \min \{ \|\hat{w}_1(t) + \hat{w}_2(t)\|, \|\hat{w}_1(t) - \hat{w}_2(t)\| \}, \quad (6)$$

whence it is evident that $\text{SALI}(t) \in [0, \sqrt{2}]$. $\text{SALI} = 0$ indicates that the two deviation vectors have become aligned in the same direction (and are equal or opposite to each other); in other words, they are linearly dependent.

Let us observe, at this point, that seeking the minimum of the two positive quantities in (6) (which are bounded above by 2) is essentially equivalent to evaluating the product

$$P(t) = \|\hat{w}_1(t) + \hat{w}_2(t)\| \cdot \|\hat{w}_1(t) - \hat{w}_2(t)\|, \quad (7)$$

at every value of t . Indeed, if the minimum of these two quantities is zero (as in the case of a chaotic reference orbit, see below), so will be the value of $P(t)$. On the other hand, if it is not zero, $P(t)$ will be proportional to the constant about which this minimum oscillates (as in the case of regular motion, see below). This suggests that, instead of computing the $\text{SALI}(t)$ from (6), one might as well evaluate the ‘exterior’ or ‘wedge’ product of the two deviation vectors $\hat{w}_1 \wedge \hat{w}_2$ for which it holds

$$\|\hat{w}_1 \wedge \hat{w}_2\| = \frac{\|\hat{w}_1 - \hat{w}_2\| \cdot \|\hat{w}_1 + \hat{w}_2\|}{2}, \quad (8)$$

and which represents the ‘area’ of the parallelogram formed by the two deviation vectors. For the definition of the wedge product see Appendix A and for a proof of (8) see Appendix B. Indeed, the ‘wedge’ product can provide much

more useful information, as it can be generalized to represent the ‘volume’ of a parallelepiped formed by the vectors $\hat{w}_1, \hat{w}_2, \dots, \hat{w}_k$, $2 \leq k \leq 2N$, regarded as deviations from an orbit of an N -degree of freedom Hamiltonian system, or a $2N$ -dimensional symplectic map.

It is the main purpose of this paper to study precisely such a generalization and reveal considerably more qualitative and quantitative information about the local and global dynamics of these systems. Before we proceed to describe this generalization, however, let us first summarize what we know about the properties of the SALI for the case of two deviation vectors \hat{w}_1, \hat{w}_2 :

- (1) In the case of chaotic orbits, the deviation vectors \hat{w}_1, \hat{w}_2 eventually become aligned in the direction of the maximal Lyapunov exponent, and $\text{SALI}(t)$ falls exponentially to zero. An analytical study of SALI’s behavior for chaotic orbits was carried out in [17] where it was shown that

$$\text{SALI}(t) \propto e^{-(\sigma_1 - \sigma_2)t} \tag{9}$$

σ_1, σ_2 being the two largest LCEs.

- (2) In the case of regular motion, on the other hand, the orbit lies on a torus and the vectors \hat{w}_1, \hat{w}_2 eventually fall on its tangent space, following a t^{-1} time evolution, having in general different directions. In this case, the SALI oscillates about values that are different from zero (for more details see [16]). This behavior is due to the fact that for regular orbits the norm of a deviation vector increases linearly in time along the flow. Thus, our normalization procedure brings about a decrease of the magnitude of the coordinates perpendicular to the torus at a rate proportional to t^{-1} and so \hat{w}_1, \hat{w}_2 eventually fall on the tangent space of the torus.

Note that in the case of 2D maps the torus is actually an invariant curve and its tangent space is 1-dimensional. So, in this case, the two unit deviation vectors eventually become linearly dependent and SALI becomes zero following a power law. This is, of course, different than the exponential decay of SALI for chaotic orbits and thus SALI can distinguish easily between the two cases even in 2D maps [15]. Thus, although the behavior of SALI in 2D maps is clearly understood, the fact remains that SALI does not always have the same behavior for regular orbits, as it may oscillate about a constant or decay to zero by a power law, depending on the dimensionality of the tangent space of the reference orbit. It might, therefore, be interesting to ask whether this index can be generalized, so that different power laws may be found to characterize regular motion in higher dimensions. It is one of the principal aims of this paper to show that such a generalization is possible.

Let us make one final remark concerning the behavior of SALI for chaotic orbits: Looking at equation (9), one might wonder what would happen in the case of a chaotic orbit whose two largest Lyapunov exponents σ_1 and

σ_2 are equal or almost equal. Although this may not be common in generic Hamiltonian systems, such cases can be found in the literature. In one such example [39], very close to a particular unstable periodic orbit of a 15 degree of freedom Hamiltonian system, the two largest Lyapunov exponents are nearly equal $\sigma_1 - \sigma_2 \approx 0.0002$. Even though, in that example, SALI still tends to zero at the rate indicated by (9), it is evident that the chaotic nature of an orbit cannot be revealed very fast by the SALI method. It is, therefore, clear that a more detailed analysis of the local dynamics is needed to further explore the properties of specific orbits, remedy the drawbacks and improve upon the advantages of the SALI. For example, if we could define an index that depends on *several* Lyapunov exponents, this might accelerate considerably the identification of chaotic motion.

3 Definition of the GALI

Let us consider an autonomous Hamiltonian system of N degrees of freedom having a Hamiltonian function

$$H(q_1, q_2, \dots, q_N, p_1, p_2, \dots, p_N) = h = \text{constant} \quad (10)$$

where q_i and p_i , $i = 1, 2, \dots, N$ are the generalized coordinates and conjugate momenta respectively. An orbit of this system is defined by a vector $\vec{x}(t) = (q_1(t), q_2(t), \dots, q_N(t), p_1(t), p_2(t), \dots, p_N(t))$, with $x_i = q_i$, $x_{i+N} = p_i$, $i = 1, 2, \dots, N$. The time evolution of this orbit is governed by Hamilton equations of motion

$$\frac{d\vec{x}}{dt} = \vec{\mathcal{V}}(\vec{x}) = \left(\frac{\partial H}{\partial \vec{p}}, -\frac{\partial H}{\partial \vec{q}} \right), \quad (11)$$

while the time evolution of an initial deviation vector $\vec{w}(0) = (dx_1(0), \dots, dx_{2N}(0))$ from the $\vec{x}(t)$ solution of (11) obeys the variational equations

$$\frac{d\vec{w}}{dt} = \mathbf{M}(\vec{x}(t)) \vec{w}, \quad (12)$$

where $\mathbf{M} = \partial \vec{\mathcal{V}} / \partial \vec{x}$ is the Jacobian matrix of $\vec{\mathcal{V}}$.

The SALI is a quantity suitable for checking whether or not two normalized deviation vectors \hat{w}_1 , \hat{w}_2 (having norm 1), eventually become linearly dependent, by falling in the same direction. The linear dependence of the two vectors is equivalent to the vanishing of the ‘area’ of the parallelogram having as edges

the two vectors. Generalizing this idea we now follow the evolution of k deviation vectors $\hat{w}_1, \hat{w}_2, \dots, \hat{w}_k$, with $2 \leq k \leq 2N$, and determine whether these eventually become linearly dependent, by checking if the ‘volume’ of the parallelepiped having these vectors as edges goes to zero. This volume will be computed as the norm of the wedge product of these vectors (see Appendix A for a definition of the wedge product).

All normalized deviation vectors $\hat{w}_i, i = 1, 2, \dots, k$, belong to the $2N$ –dimensional tangent space of the Hamiltonian flow. Using as a basis of this space the usual set of orthonormal vectors

$$\hat{e}_1 = (1, 0, 0, \dots, 0), \hat{e}_2 = (0, 1, 0, \dots, 0), \dots, \hat{e}_{2N} = (0, 0, 0, \dots, 1) \quad (13)$$

any deviation vector \hat{w}_i can be written as

$$\hat{w}_i = \sum_{j=1}^{2N} w_{ij} \hat{e}_j, \quad i = 1, 2, \dots, k \quad (14)$$

where w_{ij} are real numbers satisfying

$$\sum_{j=1}^{2N} w_{ij}^2 = 1. \quad (15)$$

Thus, equation (A.12) of Appendix A gives

$$\begin{bmatrix} \hat{w}_1 \\ \hat{w}_2 \\ \vdots \\ \hat{w}_k \end{bmatrix} = \begin{bmatrix} w_{11} & w_{12} & \cdots & w_{12N} \\ w_{21} & w_{22} & \cdots & w_{22N} \\ \vdots & \vdots & & \vdots \\ w_{k1} & w_{k2} & \cdots & w_{k2N} \end{bmatrix} \cdot \begin{bmatrix} \hat{e}_1 \\ \hat{e}_2 \\ \vdots \\ \hat{e}_{2N} \end{bmatrix}. \quad (16)$$

Using then equation (A.13) the wedge product of these k deviation vectors takes the form

$$\hat{w}_1 \wedge \hat{w}_2 \wedge \cdots \wedge \hat{w}_k = \sum_{1 \leq i_1 < i_2 < \cdots < i_k \leq 2N} \begin{vmatrix} w_{1i_1} & w_{1i_2} & \cdots & w_{1i_k} \\ w_{2i_1} & w_{2i_2} & \cdots & w_{2i_k} \\ \vdots & \vdots & & \vdots \\ w_{ki_1} & w_{ki_2} & \cdots & w_{ki_k} \end{vmatrix} \hat{e}_{i_1} \wedge \hat{e}_{i_2} \wedge \cdots \wedge \hat{e}_{i_k}, \quad (17)$$

where the sum is performed over all possible combinations of k indices out of $2N$.

If at least two of the normalized deviation vectors \hat{w}_i , $i = 1, 2, \dots, k$ are linearly dependent, all the $k \times k$ determinants appearing in equation (17) will become zero making the ‘volume’ vanish. Equivalently the quantity

$$\|\hat{w}_1 \wedge \hat{w}_2 \wedge \dots \wedge \hat{w}_k\| = \left\{ \sum_{1 \leq i_1 < i_2 < \dots < i_k \leq 2N} \begin{vmatrix} w_{1i_1} & w_{1i_2} & \dots & w_{1i_k} \\ w_{2i_1} & w_{2i_2} & \dots & w_{2i_k} \\ \vdots & \vdots & & \vdots \\ w_{ki_1} & w_{ki_2} & \dots & w_{ki_k} \end{vmatrix}^2 \right\}^{1/2} \quad (18)$$

which we shall call the ‘norm’ of the wedge product, will also become zero. Thus, we define this important quantity as the Generalized Alignment Index (GALI) of order k

$$\text{GALI}_k(t) = \|\hat{w}_1(t) \wedge \hat{w}_2(t) \wedge \dots \wedge \hat{w}_k(t)\| . \quad (19)$$

In order to compute GALI_k , therefore, we need to follow the evolution of an orbit with initial conditions $\vec{x}(0)$, using equation (11), as well as the evolution of k initially linearly independent unit deviation vectors \hat{w}_i , $i = 1, 2, \dots, k$ using the variational equations (12). At every time step, we normalize these deviation vectors to unity and compute GALI_k as the norm of their wedge product using equation (18).

Consequently, if $\text{GALI}_k(t)$ tends to zero, this would imply that the volume of the parallelepiped having the vectors \hat{w}_i as edges also shrinks to zero, as at least one of the deviation vectors becomes linearly dependent on the remaining ones. On the other hand, if $\text{GALI}_k(t)$ remains far from zero, as t grows arbitrarily, this would indicate the linear independence of the deviation vectors and the existence of a corresponding parallelepiped, whose volume is different from zero for all time.

4 Theoretical results

4.1 Exponential decay of GALI for chaotic orbits

In order to investigate the dynamics in the vicinity of a chaotic orbit of the Hamiltonian system (10) with N degrees of freedom, let us first recall

some known properties of the Lyapunov characteristic exponents, following e. g. [45,46]. It has been shown that the mean exponential rate of divergence $\sigma(\vec{x}(0), \vec{w})$ from a reference orbit with initial condition $\vec{x}(0)$ given by

$$\sigma(\vec{x}(0), \vec{w}) = \lim_{t \rightarrow \infty} \frac{1}{t} \ln \frac{\|\vec{w}(t)\|}{\|\vec{w}(0)\|} , \quad (20)$$

exists and is finite. Furthermore there is a $2N$ -dimensional basis $\{\hat{u}_1, \hat{u}_2, \dots, \hat{u}_{2N}\}$ of the tangent space of the Hamiltonian flow so that $\sigma(\vec{x}(0), \vec{w})$ takes one of the $2N$ (possibly nondistinct) values

$$\sigma_i(\vec{x}(0)) = \sigma(\vec{x}(0), \hat{u}_i) \quad , \quad i = 1, 2, \dots, 2N \quad (21)$$

which are the Lyapunov characteristic exponents, ordered in size as follows:

$$\sigma_1 \geq \sigma_2 \geq \dots \geq \sigma_{2N} . \quad (22)$$

These properties can be easily understood if the reference orbit is an unstable periodic solution of period T . In this case, the matrix \mathbf{M} of the variational equations (12) is a continuous T -periodic $2N \times 2N$ matrix. The solution of equations (12) can be written as

$$\vec{w}(t) = \mathbf{\Phi}(t) \cdot \vec{w}(0) , \quad (23)$$

where $\mathbf{\Phi}(t)$ is the so-called fundamental matrix (see e. g. [47]), such that $\mathbf{\Phi}(0) = \mathbf{I}$, the $2N \times 2N$ identity matrix. The behavior of the deviation vector $\vec{w}(t)$ and consequently the stability of the periodic orbit is determined by the eigenvalues λ_i of the so-called monodromy matrix $\mathbf{\Phi}(T)$, ordered as $|\lambda_1| \geq |\lambda_2| \geq \dots \geq |\lambda_{2N}|$. Let \hat{u}_i , $i = 1, 2, \dots, 2N$ denote the corresponding eigenvectors. Then for $\vec{w}(0) = \hat{u}_i$ we have

$$\vec{w}(nT) = \lambda_i^n \hat{u}_i \quad , \quad i = 1, 2, \dots, 2N \quad (24)$$

and from (20) we get

$$\sigma(\vec{x}(0), \hat{u}_i) = \lim_{n \rightarrow \infty} \frac{1}{nT} \ln |\lambda_i^n| = \frac{\ln |\lambda_i|}{T} \quad , \quad i = 1, 2, \dots, 2N. \quad (25)$$

Furthermore, if we write

$$\vec{w}(0) = \sum_{i=1}^{2N} c_i \hat{u}_i , \quad (26)$$

it follows from (24) that the first nonvanishing coefficient c_i dominates the subsequent evolution of $\vec{w}(nT)$. Thus, if $c_1 \neq 0$ we get from (20) $\sigma(\vec{x}(0), \vec{w}) = \sigma_1$, if $c_1 = 0$ and $c_2 \neq 0$ we get $\sigma(\vec{x}(0), \vec{w}) = \sigma_2$ and so on. So, the evolution of the initial deviation vector $\vec{w}(0)$ is well approximated by

$$\vec{w}(nT) = \sum_{i=1}^{2N} c_i e^{\sigma_i nT} \hat{u}_i, \quad (27)$$

For a nonperiodic orbit we cannot define such eigenvalues and eigenvectors as above. Nevertheless, Oseledec [1] has proven the existence of basis vectors $\{\hat{u}_1, \hat{u}_2, \dots, \hat{u}_{2N}\}$ and Lyapunov exponents for nonperiodic orbits. This is perhaps not surprising, since periodic orbits are dense in the phase space of Hamiltonian systems and thus a periodic orbit of arbitrary large period can always be found arbitrary close to any nonperiodic orbit. So, the time evolution of a deviation vector may be approximated by a variant of equation (27), i. e.

$$\vec{w}(t) = \sum_{i=1}^{2N} c_i e^{d_i t} \hat{u}_i, \quad (28)$$

where c_i, d_i are real numbers depending on the specific phase space location through which the reference orbit passes. Thus, the quantities $d_i, i = 1, 2, \dots, 2N$ may be thought of as ‘local Lyapunov exponents’ having as limits for $t \rightarrow \infty$ the ‘global’ LCEs $\sigma_i, i = 1, 2, \dots, 2N$. We notice that even if in some special cases where the vectors $\hat{u}_i, i = 1, 2, \dots, 2N$ are known a priori, so that one could set $\vec{w}(0) = \hat{u}_i$, the computational errors in the numerical evolution of the deviation vector would lead to the actual computation of σ_1 from equation (1) [5].

It is well known that Hamiltonian systems are generically non-integrable and possess Lyapunov exponents in chaotic domains which are real and grouped in pairs of opposite sign with two of them being equal to zero. We, therefore, have $\sigma_i = -\sigma_{2N-i+1}$ for $i = 1, 2, \dots, N$ and $\sigma_1 \geq \sigma_2 \geq \dots \geq \sigma_{N-1} \geq \sigma_N = \sigma_{N+1} = 0 \geq \sigma_{N+2} \geq \dots \geq \sigma_{2N}$. Assuming that, after a certain time interval, the $d_i, i = 1, 2, \dots, 2N$ do not fluctuate significantly about their limiting values, we write $d_i \approx \sigma_i$ and express the evolution of the deviation vectors \vec{w}_i in the form

$$\vec{w}_i(t) = \sum_{j=1}^{2N} c_j^i e^{\sigma_j t} \hat{u}_j \quad (29)$$

(see discussion in section 5.1 and figure 1). Thus, if $\sigma_1 > \sigma_2$, a leading order estimate of the deviation vector’s Euclidean norm (for t large enough), is given

by

$$\|\vec{w}_i(t)\| \approx |c_1^i| e^{\sigma_1 t}. \quad (30)$$

Consequently, the matrix \mathbf{C} in (A.12) of coefficients of k normalized deviation vectors $\hat{w}_i(t) = \vec{w}_i(t)/\|\vec{w}_i(t)\|$, $i = 1, 2, \dots, k$ with $2 \leq k \leq 2N$, using as basis of the vector space the set $\{\hat{u}_1, \hat{u}_2, \dots, \hat{u}_{2N}\}$ becomes

$$\mathbf{C}(t) = [c_{ij}] = \begin{bmatrix} s_1 \frac{c_2^1}{|c_1^1|} e^{-(\sigma_1 - \sigma_2)t} & \frac{c_3^1}{|c_1^1|} e^{-(\sigma_1 - \sigma_3)t} & \dots & \frac{c_{2N}^1}{|c_1^1|} e^{-(\sigma_1 - \sigma_{2N})t} \\ s_2 \frac{c_2^2}{|c_1^2|} e^{-(\sigma_1 - \sigma_2)t} & \frac{c_3^2}{|c_1^2|} e^{-(\sigma_1 - \sigma_3)t} & \dots & \frac{c_{2N}^2}{|c_1^2|} e^{-(\sigma_1 - \sigma_{2N})t} \\ \vdots & \vdots & \vdots & \vdots \\ s_k \frac{c_2^k}{|c_1^k|} e^{-(\sigma_1 - \sigma_2)t} & \frac{c_3^k}{|c_1^k|} e^{-(\sigma_1 - \sigma_3)t} & \dots & \frac{c_{2N}^k}{|c_1^k|} e^{-(\sigma_1 - \sigma_{2N})t} \end{bmatrix}, \quad (31)$$

with $s_i = \text{sign}(c_1^i)$ and $i = 1, 2, \dots, k$, $j = 1, 2, \dots, 2N$ and so we have

$$\begin{bmatrix} \hat{w}_1 & \hat{w}_2 & \dots & \hat{w}_k \end{bmatrix}^T = \mathbf{C} \cdot \begin{bmatrix} \hat{u}_1 & \hat{u}_2 & \dots & \hat{u}_{2N} \end{bmatrix}^T \quad (32)$$

with (T) denoting the transpose of a matrix. The wedge product of the k normalized deviation vectors is then computed as in equation (17) by:

$$\hat{w}_1(t) \wedge \hat{w}_2(t) \wedge \dots \wedge \hat{w}_k(t) = \sum_{1 \leq i_1 < i_2 < \dots < i_k \leq 2N} \begin{vmatrix} c_{1i_1} & c_{1i_2} & \dots & c_{1i_k} \\ c_{2i_1} & c_{2i_2} & \dots & c_{2i_k} \\ \vdots & \vdots & \ddots & \vdots \\ c_{ki_1} & c_{ki_2} & \dots & c_{ki_k} \end{vmatrix} \hat{u}_{i_1} \wedge \hat{u}_{i_2} \wedge \dots \wedge \hat{u}_{i_k}. \quad (33)$$

Note that the quantity

$$S_k = \left\{ \sum_{1 \leq i_1 < i_2 < \dots < i_k \leq 2N} \begin{vmatrix} c_{1i_1} & c_{1i_2} & \dots & c_{1i_k} \\ c_{2i_1} & c_{2i_2} & \dots & c_{2i_k} \\ \vdots & \vdots & \ddots & \vdots \\ c_{ki_1} & c_{ki_2} & \dots & c_{ki_k} \end{vmatrix}^2 \right\}^{1/2} \quad (34)$$

is *not identical* to the norm (18) of the k -vector $\hat{w}_1(t) \wedge \hat{w}_2(t) \wedge \dots \wedge \hat{w}_k(t)$ as the wedge product in equation (33) is not expressed with respect to the basis

(13). Thus one should consider the transformation

$$\begin{bmatrix} \hat{u}_1 & \hat{u}_2 & \dots & \hat{u}_{2N} \end{bmatrix}^T = \mathbf{T}_c \cdot \begin{bmatrix} \hat{e}_1 & \hat{e}_2 & \dots & \hat{e}_{2N} \end{bmatrix}^T, \quad (35)$$

between the two bases, with \mathbf{T}_c denoting the transformation matrix. Of course, when considering the wedge product of $2N$ deviation vectors one can easily show that

$$\|\hat{w}_1 \wedge \hat{w}_2 \wedge \dots \wedge \hat{w}_{2N}\| = S_{2N} \cdot |\det \mathbf{T}_c|. \quad (36)$$

If, on the other hand, we consider the wedge product of *fewer* than $2N$ deviation vectors, the norm (18) and the quantity S_k (34) are not related through a simple expression like (36). We shall proceed, however, to obtain results using (34) instead of (18), as we do not expect that such a change of basis will affect significantly the dynamics and alter our conclusions for the following reasons: First, we note that both quantities are zero when at least two of the k deviation vectors are linearly dependent, due to the fact that all the determinants appearing in equations (18) and (34) vanish. In addition, the transformation matrix \mathbf{T}_c is not singular as the sets $\{\hat{u}_i\}$ and $\{\hat{e}_i\}$, $i = 1, 2, \dots, 2N$ continue to be valid bases of the vector space. Thus, both quantities are expected to behave in a similar way in the case of chaotic orbits, where the deviation vectors tend to become linearly dependent. Thus, by studying analytically the time evolution of S_k through (34), we expect to derive accurate approximations of the behavior of the GALI_k (19) for chaotic orbits. The validity of this approximation is numerically tested and verified in section 5.

Let us now see how this approximation is derived: The determinants appearing in the definition of S_k (see equation (34)) can be divided in two categories depending on whether or not they contain the first column of matrix \mathbf{C} . Using standard properties of determinants, we see that those that do contain the first column yield

$$D_{1,j_1,j_2,\dots,j_{k-1}} = \begin{vmatrix} s_1 \frac{c_{j_1}^1}{|c_1^1|} e^{-(\sigma_1 - \sigma_{j_1})t} & \dots & \frac{c_{j_{k-1}}^1}{|c_1^1|} e^{-(\sigma_1 - \sigma_{j_{k-1}})t} \\ s_2 \frac{c_{j_1}^2}{|c_1^2|} e^{-(\sigma_1 - \sigma_{j_1})t} & \dots & \frac{c_{j_{k-1}}^2}{|c_1^2|} e^{-(\sigma_1 - \sigma_{j_{k-1}})t} \\ \vdots & & \vdots \\ s_k \frac{c_{j_1}^k}{|c_1^k|} e^{-(\sigma_1 - \sigma_{j_1})t} & \dots & \frac{c_{j_{k-1}}^k}{|c_1^k|} e^{-(\sigma_1 - \sigma_{j_{k-1}})t} \end{vmatrix} =$$

$$= \begin{vmatrix} s_1 \frac{c_{j_1}^1}{|c_1^1|} & \cdots & \frac{c_{j_{k-1}}^1}{|c_1^1|} \\ s_2 \frac{c_{j_1}^2}{|c_1^2|} & \cdots & \frac{c_{j_{k-1}}^2}{|c_1^2|} \\ \vdots & & \vdots \\ s_k \frac{c_{j_1}^k}{|c_1^k|} & \cdots & \frac{c_{j_{k-1}}^k}{|c_1^k|} \end{vmatrix} e^{-[(\sigma_1 - \sigma_{j_1}) + (\sigma_1 - \sigma_{j_2}) + \cdots + (\sigma_1 - \sigma_{j_{k-1}})]t} \quad (37)$$

with $1 < j_1 < j_2 < \cdots < j_{k-1} \leq 2N$. Thus, the time evolution of $D_{1,j_1,j_2,\dots,j_{k-1}}$ is mainly determined by the exponential law

$$D_{1,j_1,j_2,\dots,j_{k-1}} \propto e^{-[(\sigma_1 - \sigma_{j_1}) + (\sigma_1 - \sigma_{j_2}) + \cdots + (\sigma_1 - \sigma_{j_{k-1}})]t}. \quad (38)$$

Similarly, we deduce that the determinants that *do not* contain the first column of matrix \mathbf{C} (31) have the form

$$D_{j_1,j_2,\dots,j_k} = \begin{vmatrix} \frac{c_{j_1}^1}{|c_1^1|} e^{-(\sigma_1 - \sigma_{j_1})t} & \frac{c_{j_2}^1}{|c_1^1|} e^{-(\sigma_1 - \sigma_{j_2})t} & \cdots & \frac{c_{j_k}^1}{|c_1^1|} e^{-(\sigma_1 - \sigma_{j_k})t} \\ \frac{c_{j_1}^2}{|c_1^2|} e^{-(\sigma_1 - \sigma_{j_1})t} & \frac{c_{j_2}^2}{|c_1^2|} e^{-(\sigma_1 - \sigma_{j_2})t} & \cdots & \frac{c_{j_k}^2}{|c_1^2|} e^{-(\sigma_1 - \sigma_{j_k})t} \\ \vdots & \vdots & & \vdots \\ \frac{c_{j_1}^k}{|c_1^k|} e^{-(\sigma_1 - \sigma_{j_1})t} & \frac{c_{j_2}^k}{|c_1^k|} e^{-(\sigma_1 - \sigma_{j_2})t} & \cdots & \frac{c_{j_k}^k}{|c_1^k|} e^{-(\sigma_1 - \sigma_{j_k})t} \end{vmatrix} =$$

$$= \begin{vmatrix} \frac{c_{j_1}^1}{|c_1^1|} & \frac{c_{j_2}^1}{|c_1^1|} & \cdots & \frac{c_{j_k}^1}{|c_1^1|} \\ \frac{c_{j_1}^2}{|c_1^2|} & \frac{c_{j_2}^2}{|c_1^2|} & \cdots & \frac{c_{j_k}^2}{|c_1^2|} \\ \vdots & \vdots & & \vdots \\ \frac{c_{j_1}^k}{|c_1^k|} & \frac{c_{j_2}^k}{|c_1^k|} & \cdots & \frac{c_{j_k}^k}{|c_1^k|} \end{vmatrix} e^{-[(\sigma_1 - \sigma_{j_1}) + (\sigma_1 - \sigma_{j_2}) + \cdots + (\sigma_1 - \sigma_{j_{k-1}}) + (\sigma_1 - \sigma_{j_k})]t} \quad (39)$$

with $1 < j_1 < j_2 < \cdots < j_{k-1} < j_k \leq 2N$. Thus, the values of these determinants also tend to zero following an exponential law

$$D_{j_1,j_2,\dots,j_k} \propto e^{-[(\sigma_1 - \sigma_{j_1}) + (\sigma_1 - \sigma_{j_2}) + \cdots + (\sigma_1 - \sigma_{j_{k-1}}) + (\sigma_1 - \sigma_{j_k})]t}. \quad (40)$$

Clearly, from all determinants appearing in the definition of S_k , (34), the one that decreases the *slowest* is the one containing the first k columns of matrix \mathbf{C} in (31):

$$D_{1,2,3,\dots,k} \propto e^{-[(\sigma_1 - \sigma_2) + (\sigma_1 - \sigma_3) + \cdots + (\sigma_1 - \sigma_k)]t}. \quad (41)$$

All other determinants appearing in equations (38) and (40) tend to zero *faster* than $D_{1,2,3,\dots,k}$ since the quantities in their exponentials are smaller or equal

to the exponent in (41). We, therefore, conclude that the rate of decrease of S_k is dominated by (41), yielding the approximation

$$S_k(t) \propto e^{-[(\sigma_1 - \sigma_2) + (\sigma_1 - \sigma_3) + \dots + (\sigma_1 - \sigma_k)]t}. \quad (42)$$

Furthermore, since the norm (18) of the k -vector $\hat{w}_1 \wedge \hat{w}_2 \wedge \dots \wedge \hat{w}_k$ is expected to evolve in a similar way as S_k , we conclude that GALI_k tends to zero in the same manner as above, i.e.

$$\text{GALI}_k(t) \propto e^{-[(\sigma_1 - \sigma_2) + (\sigma_1 - \sigma_3) + \dots + (\sigma_1 - \sigma_k)]t}. \quad (43)$$

We note here that in [17], where it was shown theoretically that SALI tends exponentially to zero for chaotic orbits as $\text{SALI}(t) \propto \exp\{-(\sigma_1 - \sigma_2)t\}$ (which is equivalent to equation (43) for $k = 2$), equation (29) was also retrieved, although it was wrongly assumed that the LCEs are related to the eigenvalues of matrix \mathbf{M} of the variational equations (12).

In the previous analysis we assumed that $\sigma_1 > \sigma_2$ so that the norm of each deviation vector can be well approximated by equation (30). If the first m Lyapunov exponents, with $1 < m < k$, are equal, or very close to each other, i.e. $\sigma_1 \simeq \sigma_2 \simeq \dots \simeq \sigma_m$ equation (43) becomes

$$\text{GALI}_k(t) \propto e^{-[(\sigma_1 - \sigma_{m+1}) + (\sigma_1 - \sigma_{m+2}) + \dots + (\sigma_1 - \sigma_k)]t}, \quad (44)$$

which still describes an exponential decay. However, for $k \leq m < N$ the GALI_k does not tend to zero as there exists at least one determinant of the matrix \mathbf{C} that does not vanish. In this case, of course, one should increase the number of deviation vectors until an exponential decrease of GALI_k is achieved. The extreme situation that all $\sigma_i = 0$ corresponds to motion on quasiperiodic tori, where all orbits are regular and is described below.

4.2 The evaluation of GALI for regular orbits

As is well-known, regular orbits of an N degree of freedom Hamiltonian system (10) typically lie on N -dimensional tori. If such tori are found around a stable periodic orbit, they can be accurately described by N formal integrals of motion in involution, so that the system would appear locally integrable. This means that we could perform a local transformation to action-angle variables, considering as actions J_1, J_2, \dots, J_N the values of the N formal integrals, so

that Hamilton's equations of motion, locally attain the form

$$\begin{aligned} \dot{J}_i &= 0 \\ \dot{\theta}_i &= \omega_i(J_1, J_2, \dots, J_N) \end{aligned} \quad i = 1, 2, \dots, N. \quad (45)$$

These can be easily integrated to give

$$\begin{aligned} J_i(t) &= J_{i0} \\ \theta_i(t) &= \theta_{i0} + \omega_i(J_{10}, J_{20}, \dots, J_{N0}) t \end{aligned} \quad i = 1, 2, \dots, N, \quad (46)$$

where $J_{i0}, \theta_{i0}, i = 1, 2, \dots, N$ are the initial conditions.

By denoting as $\xi_i, \eta_i, i = 1, 2, \dots, N$ small deviations of J_i and θ_i respectively, the variational equations of system (45), describing the evolution of a deviation vector are

$$\begin{aligned} \dot{\xi}_i &= 0 \\ \dot{\eta}_i &= \sum_{j=1}^N \omega_{ij} \cdot \xi_j \end{aligned} \quad i = 1, 2, \dots, N, \quad (47)$$

where

$$\omega_{ij} = \left. \frac{\partial \omega_i}{\partial J_j} \right|_{\vec{J}_0} \quad i, j = 1, 2, \dots, N, \quad (48)$$

and $\vec{J}_0 = (J_{10}, J_{20}, \dots, J_{N0}) = \text{constant}$, represents the N -dimensional vector of the initial actions. The solution of these equations is:

$$\begin{aligned} \xi_i(t) &= \xi_i(0) \\ \eta_i(t) &= \eta_i(0) + \left[\sum_{j=1}^N \omega_{ij} \xi_j(0) \right] t \end{aligned} \quad i = 1, 2, \dots, N. \quad (49)$$

From equations (49) we see that an initial deviation vector $\vec{w}(0)$ with coordinates $\xi_i(0), i = 1, 2, \dots, N$ in the action variables and $\eta_i(0), i = 1, 2, \dots, N$ in the angles, i. e. $\vec{w}(0) = (\xi_1(0), \xi_2(0), \dots, \xi_N(0), \eta_1(0), \eta_2(0), \dots, \eta_N(0))$, evolves in time in such a way that its action coordinates remain constant, while its angle coordinates increase linearly in time. This behavior implies an almost linear increase of the norm of the deviation vector. To see this, let us assume that initially this vector $\vec{w}(0)$ has unit magnitude, i. e.

$$\sum_{i=1}^N \xi_i(0)^2 + \sum_{i=1}^N \eta_i(0)^2 = 1 \quad (50)$$

whence the time evolution of its norm is given by

$$\|\vec{w}(t)\| = \left\{ 1 + \left[\sum_{i=1}^N \left(\sum_{j=1}^N \omega_{ij} \xi_j(0) \right)^2 \right] t^2 + \left[2 \sum_{i=1}^N \left(\eta_i(0) \sum_{j=1}^N \omega_{ij} \xi_j(0) \right) \right] t \right\}^{1/2}, \quad (51)$$

while the normalized deviation vector $\hat{w}(t)$ becomes:

$$\hat{w}(t) = \frac{1}{\|\vec{w}(t)\|} \left(\xi_1(0), \dots, \xi_N(0), \eta_1(0) + \left[\sum_{j=1}^N \omega_{1j} \xi_j(0) \right] t, \dots, \eta_N(0) + \left[\sum_{j=1}^N \omega_{Nj} \xi_j(0) \right] t \right). \quad (52)$$

Since the norm (51) of a deviation vector, for t large enough, increases practically linearly with t , the normalized deviation vector (52) tends to fall on the tangent space of the torus, since its coordinates perpendicular to the torus (i. e. the coordinates along the action directions) vanish following a t^{-1} rate. This behavior has already been shown numerically in the case of an integrable Hamiltonian of 2 degrees of freedom in [16].

Using as a basis of the $2N$ -dimensional tangent space of the Hamiltonian flow the $2N$ unit vectors $\{\hat{v}_1, \hat{v}_2, \dots, \hat{v}_{2N}\}$, such that the first N of them, $\hat{v}_1, \hat{v}_2, \dots, \hat{v}_N$ correspond to the N action variables and the remaining ones, $\hat{v}_{N+1}, \hat{v}_{N+2}, \dots, \hat{v}_{2N}$ to the N conjugate angle variables, any unit deviation vector \hat{w}_i , $i = 1, 2, \dots$ can be written as

$$\hat{w}_i(t) = \frac{1}{\|\vec{w}(t)\|} \left[\sum_{j=1}^N \xi_j^i(0) \hat{v}_j + \sum_{j=1}^N \left(\eta_j^i(0) + \sum_{k=1}^N \omega_{kj} \xi_j^i(0) t \right) \hat{v}_{N+j} \right]. \quad (53)$$

We point out that the quantities ω_{ij} , $i, j = 1, 2, \dots, N$, in (48), depend only on the particular reference orbit and not on the choice of the deviation vector. We also note that the basis \hat{w}_i , $i = 1, 2, \dots, 2N$ depends on the specific torus on which the motion occurs and is related to the usual vector basis \hat{e}_i , $i = 1, 2, \dots, 2N$ of equation (13), through a non-singular transformation, similar to the one of equation (35), having the form:

$$\left[\hat{v}_1 \ \hat{v}_2 \ \dots \ \hat{v}_{2N} \right]^T = \mathbf{T}_o \cdot \left[\hat{e}_1 \ \hat{e}_2 \ \dots \ \hat{e}_{2N} \right]^T \quad (54)$$

with \mathbf{T}_o denoting the transformation matrix. The basis $\{\hat{e}_1, \hat{e}_2, \dots, \hat{e}_{2N}\}$ is used to describe the evolution of a deviation vector with respect to the original q_i , p_i $i = 1, 2, \dots, N$ coordinates of the Hamiltonian system (10), while the basis $\{\hat{v}_1, \hat{v}_2, \dots, \hat{v}_{2N}\}$ is used to describe the same evolution, if we consider the original system in action-angle variables, so that the equations of motion are the ones given by (45).

Defining then by $\boldsymbol{\xi}_i^{0,k}$ and $\boldsymbol{\eta}_i^k$ the $k \times 1$ column matrices

$$\boldsymbol{\xi}_i^{0,k} = \left[\xi_i^1(0) \ \xi_i^2(0) \ \dots \ \xi_i^k(0) \right]^T, \quad \boldsymbol{\eta}_i^k = \left[\eta_i^1(0) \ \eta_i^2(0) \ \dots \ \eta_i^k(0) \right]^T, \quad (62)$$

the matrix \mathbf{D} of (60) assumes the much simpler form

$$\begin{aligned} \mathbf{D}(t) &= \frac{1}{\prod_{i=1}^k M_i(t)} \cdot \left[\boldsymbol{\xi}_1^{0,k} \ \dots \ \boldsymbol{\xi}_N^{0,k} \ \boldsymbol{\eta}_1^k + \sum_{i=1}^N \omega_{1i} \boldsymbol{\xi}_i^{0,k} t \ \dots \ \boldsymbol{\eta}_N^k + \sum_{i=1}^N \omega_{Ni} \boldsymbol{\xi}_i^{0,k} t \right] = \\ &= \frac{1}{\prod_{i=1}^k M_i(t)} \cdot \mathbf{D}^{0,k}(t). \end{aligned} \quad (63)$$

Suppose now that we have m linearly independent deviation vectors, with $m \leq k$ and $m \leq N$, initially located in the tangent space of the torus and let them be the first m deviation vectors in equation (59). This implies, in the above notation, that the $\boldsymbol{\xi}_i$ vectors in (63) now have the form

$$\boldsymbol{\xi}_i^{m,k} = \left[0 \ 0 \ \dots \ 0 \ \xi_i^{m+1}(0) \ \xi_i^{m+2}(0) \ \dots \ \xi_i^k(0) \right]^T \quad (64)$$

where the first superscript, m , refers to the number of first components being equal to zero. Thus, the matrix \mathbf{D} of (63) in this case reads

$$\begin{aligned} \mathbf{D}(t) &= \frac{1}{\prod_{i=1}^{k-m} M_{m+i}(t)} \cdot \left[\boldsymbol{\xi}_1^{m,k} \ \dots \ \boldsymbol{\xi}_N^{m,k} \ \boldsymbol{\eta}_1^k + \sum_{i=1}^N \omega_{1i} \boldsymbol{\xi}_i^{m,k} t \ \dots \ \boldsymbol{\eta}_N^k + \sum_{i=1}^N \omega_{Ni} \boldsymbol{\xi}_i^{m,k} t \right] = \\ &= \frac{1}{\prod_{i=1}^{k-m} M_{m+i}(t)} \cdot \mathbf{D}^{m,k}(t), \end{aligned} \quad (65)$$

where the first superscript of $\mathbf{D}^{m,k}(t)$ in equations (63) and (65) has an analogous meaning as in the $\boldsymbol{\xi}_i^{m,k}$. We note that for $k = m$ we define $\prod_{i=1}^0 M_{m+i}(t) = 1$.

Using again equation (A.13), we write the wedge product of the k normalized deviation vectors as

$$\hat{w}_1(t) \wedge \hat{w}_2(t) \wedge \dots \wedge \hat{w}_k(t) = \sum_{1 \leq i_1 < i_2 < \dots < i_k \leq 2N} \begin{vmatrix} d_{1i_1} & d_{1i_2} & \dots & d_{1i_k} \\ d_{2i_1} & d_{2i_2} & \dots & d_{2i_k} \\ \vdots & \vdots & & \vdots \\ d_{ki_1} & d_{ki_2} & \dots & d_{ki_k} \end{vmatrix} \hat{u}_{i_1} \wedge \hat{u}_{i_2} \wedge \dots \wedge \hat{u}_{i_k}. \quad (66)$$

and introduce the analogous quantity

$$S'_k = \left\{ \sum_{1 \leq i_1 < i_2 < \dots < i_k \leq 2N} \begin{vmatrix} d_{1i_1} & d_{1i_2} & \dots & d_{1i_k} \\ d_{2i_1} & d_{2i_2} & \dots & d_{2i_k} \\ \vdots & \vdots & & \vdots \\ d_{ki_1} & d_{ki_2} & \dots & d_{ki_k} \end{vmatrix}^2 \right\}^{1/2}. \quad (67)$$

as in the case of chaotic orbits, see (33) and (34) respectively.

As we have already explained, the k deviation vectors will eventually fall on the N -dimensional tangent space of the torus on which the motion occurs. Of course, if some of them are already located in the tangent space, at $t = 0$, they will remain there forever. In their final state, the deviation vectors will have coordinates only in the N -dimensional space spanned by $\hat{v}_{N+1}, \hat{v}_{N+2}, \dots, \hat{v}_{2N}$. Now, if we start with $2 \leq k \leq N$ general deviation vectors there is no particular reason for them to become linearly dependent and their wedge product will be different from zero, yielding S'_k and GALI_k which are *not zero*. However, if we start with $N < k \leq 2N$ deviation vectors, some of them will necessarily become linearly dependent. Thus, in this case, their wedge product (as well as S'_k and GALI_k) will be zero.

We, therefore, need to examine in more detail the behavior of these S'_k . Since, in general, we choose the initial deviation vectors randomly (insisting only that they be linearly independent), the most common situation is that none of the initial deviation vectors is tangent to the torus. However, as we are not certain that this will always hold, let us suppose that $0 < m \leq N$ of our deviation vectors are initially in the tangent space of the torus. For $2 \leq k \leq N$, this will make no difference, as the GALI_k tends to a non-zero constant. However, for $N < k \leq 2N$, GALI_k goes to zero by a power law and the fact that m vectors are already in the tangent space, at $t = 0$, may significantly affect the decay rate of the index. Thus, in such cases, the behavior of GALI needs to be treated separately.

4.2.1 The case of $m = 0$ tangent initial deviation vectors

Let us consider first the most general case that *no* deviation vector is initially tangent to the torus. In this case, the matrix \mathbf{D} , whose elements appear in the definition of S'_k , has the form given in equation (63). So all determinants appearing in the definition of S'_k have as a common factor the quantity $1/\prod_{i=1}^k M_i(t)$, which, due to (61), decreases to zero according to the power

law

$$\frac{1}{\prod_{i=1}^k M_i(t)} \propto \frac{1}{t^k}. \quad (68)$$

In order to determine the precise time evolution of S'_k , we search for the fastest increasing determinants of all the possible $k \times k$ minors of the matrix $\mathbf{D}^{0,k}$, in (63), as time t grows.

Let us start with k being less than or equal to the dimension of the tangent space of the torus, i. e. $2 \leq k \leq N$. The fastest increasing determinants in this case are the $N!/(k!(N-k)!)$ determinants, whose k columns are chosen among the last N columns of matrix $\mathbf{D}^{0,k}$:

$$\Delta_{j_1, j_2, \dots, j_k}^{0,k} = \left| \boldsymbol{\eta}_{j_1}^k + \sum_{i=1}^N \omega_{j_1 i} \boldsymbol{\xi}_i^{0,k} t \boldsymbol{\eta}_{j_2}^k + \sum_{i=1}^N \omega_{j_2 i} \boldsymbol{\xi}_i^{0,k} t \cdots \boldsymbol{\eta}_{j_k}^k + \sum_{i=1}^N \omega_{j_k i} \boldsymbol{\xi}_i^{0,k} t \right|, \quad (69)$$

with $1 \leq j_1 < j_2 < \dots < j_k \leq N$. Using standard properties of determinants, we easily see that the time evolution of $\Delta_{j_1, j_2, \dots, j_k}^{0,k}$ is mainly determined by the behavior of determinants of the form

$$\left| \omega_{j_1 m_1} \boldsymbol{\xi}_{m_1}^{0,k} t \omega_{j_2 m_2} \boldsymbol{\xi}_{m_2}^{0,k} t \cdots \omega_{j_k m_k} \boldsymbol{\xi}_{m_k}^{0,k} t \right| = t^k \prod_{i=1}^k \omega_{j_i m_i} \cdot \left| \boldsymbol{\xi}_{m_1}^{0,k} \boldsymbol{\xi}_{m_2}^{0,k} \cdots \boldsymbol{\xi}_{m_k}^{0,k} \right| \propto t^k, \quad (70)$$

where $m_i \in \{1, 2, \dots, N\}$, $i = 1, 2, \dots, k$, with $m_i \neq m_j$, for all $i \neq j$. Thus, from (68) and (70) we conclude that the contribution to the behavior of S'_k of the determinants related to $\Delta_{j_1, j_2, \dots, j_k}^{0,k}$ is to provide constant terms in (67). All other determinants appearing in the definition of S'_k , not being of the form of $\Delta_{j_1, j_2, \dots, j_k}^{0,k}$, contain at least one column from the first N columns of matrix $\mathbf{D}^{0,k}$ and introduce in (67) terms that grow at a rate *slower* than t^k , which will ultimately have no bearing on the behavior of $\text{GALI}_k(t)$. To see this, let us consider a particular determinant of this kind

$$\Delta_m^{0,k} = \left| \boldsymbol{\xi}_1^{0,k} \cdots \boldsymbol{\xi}_m^{0,k} \boldsymbol{\eta}_1^k + \sum_{i=1}^N \omega_{1i} \boldsymbol{\xi}_i^{0,k} t \cdots \boldsymbol{\eta}_{k-m}^k + \sum_{i=1}^N \omega_{k-m i} \boldsymbol{\xi}_i^{0,k} t \right|, \quad (71)$$

containing the first m columns of matrix $\mathbf{D}^{0,k}$, which are related to the action coordinates of the system, and the first $k-m$ columns of the angle related columns of $\mathbf{D}^{0,k}$, with $1 \leq m \leq k$. The first m columns of $\Delta_m^{0,k}$ are time independent. Using repeatedly a standard property of determinants, we easily see that the time evolution of $\Delta_m^{0,k}$ is mainly determined by the time evolution of determinants of the form:

$$\left| \boldsymbol{\xi}_1^{0,k} \boldsymbol{\xi}_2^{0,k} \cdots \boldsymbol{\xi}_m^{0,k} \omega_{1i_1} \boldsymbol{\xi}_{i_1}^{0,k} t \omega_{2i_2} \boldsymbol{\xi}_{i_2}^{0,k} t \cdots \omega_{k-m i_{k-m}} \boldsymbol{\xi}_{i_{k-m}}^{0,k} t \right| \propto t^{k-m}, \quad (72)$$

with $i_j \in \{m+1, m+2, \dots, N\}$, $j = 1, 2, \dots, k-m$ and $i_j \neq i_l$, for all $j \neq l$. Thus, the contribution to the behavior of S'_k of determinants similar to $\Delta_m^{0,k}$ are terms proportional to $t^{k-m}/t^k = 1/t^m$ ($1 \leq m \leq k$), tending to zero as t grows. Since the $k \times k$ determinants appearing in the definition of S'_k involve both terms of the form (69), growing as t^k and of the form (71), growing as t^{k-m} , the overall behavior of S'_k will be defined by determinants growing as t^k , which when combined with (68) yields the important result

$$\text{GALI}_k(t) \approx \text{constant for } 2 \leq k \leq N. \quad (73)$$

Next, let us now turn to the case of k deviation vectors with $N < k \leq 2N$. The fastest growing determinants are again those containing the last N columns of the matrix $\mathbf{D}^{0,k}$:

$$\Delta_{j_1, j_2, \dots, j_{k-N}, 1, 2, \dots, N}^{0,k} = \left| \boldsymbol{\xi}_{j_1}^{0,k} \cdots \boldsymbol{\xi}_{j_{k-N}}^{0,k} \boldsymbol{\eta}_1^k + \sum_{i=1}^N \omega_{1i} \boldsymbol{\xi}_i^{0,k} t \cdots \boldsymbol{\eta}_N^k + \sum_{i=1}^N \omega_{Ni} \boldsymbol{\xi}_i^{0,k} t \right|, \quad (74)$$

with $1 \leq j_1 < j_2 < \dots < j_{k-N} \leq N$. The first $k-N$ columns of $\Delta_{j_1, j_2, \dots, j_{k-N}, 1, 2, \dots, N}^{0,k}$ are chosen among the first N columns of $\mathbf{D}^{0,k}$ which are time independent. So there exist $N!/((k-N)!(2N-k)!)$ determinants of the form (74), which can be written as a sum of simpler $k \times k$ determinants, each containing in the position of its last N columns $\boldsymbol{\eta}_i^k$, $i = 1, 2, \dots, N$ and/or columns of the form $\omega_{ji} \boldsymbol{\xi}_i^{0,k} t$ with $i, j = 1, 2, \dots, N$. We exclude the ones where $\boldsymbol{\xi}_i^{0,k}$, $i = 1, 2, \dots, N$ appear more than once, since in that case the corresponding determinant is zero. Among the remaining determinants, the fastest increasing ones are those containing as many columns proportional to t as possible.

Since t is always multiplied by the $\boldsymbol{\xi}_i^{0,k}$, and such columns occupy the first $k-N$ columns of $\Delta_{j_1, j_2, \dots, j_{k-N}, 1, 2, \dots, N}^{0,k}$, t appears at most $N - (k-N) = 2N - k$ times. Otherwise the determinant would contain the same $\boldsymbol{\xi}_i^{0,k}$ column at least twice and would be equal to zero. The remaining $k - (2N - k) - (k - N) = k - N$ columns are filled by the $\boldsymbol{\eta}_i^k$ each of which appears at most once. Thus, the time evolution of $\Delta_{j_1, j_2, \dots, j_{k-N}, 1, 2, \dots, N}^{0,k}$ is mainly determined by determinants of the form:

$$\left| \boldsymbol{\xi}_{j_1}^{0,k} \cdots \boldsymbol{\xi}_{j_{k-N}}^{0,k} \boldsymbol{\eta}_{i_1}^{0,k} \cdots \boldsymbol{\eta}_{i_{k-N}}^{0,k} \omega_{i_{k-N+1} m_1} \boldsymbol{\xi}_{m_1}^{0,k} t \cdots \omega_{i_N m_{2N-k}} \boldsymbol{\xi}_{i_{2N-k}}^{0,k} t \right| \propto t^{2N-k}, \quad (75)$$

with $i_l \in \{1, 2, \dots, N\}$, $l = 1, 2, \dots, N$, $i_l \neq i_j$, for all $l \neq j$ and $m_l \in \{1, 2, \dots, N\}$, $l = 1, 2, \dots, 2N - k$, $m_l \notin \{j_1, j_2, \dots, j_{k-N}\}$, $m_l \neq m_j$, for all $l \neq j$. So determinants of the form (74) contribute to the time evolution of S'_k by introducing terms proportional to $t^{2N-k}/t^k = 1/t^{2(k-N)}$. All other determinants appearing in the definition of S'_k , not having the form of $\Delta_{j_1, j_2, \dots, j_{k-N}, 1, 2, \dots, N}^{0,k}$, introduce terms that tend to zero faster than $1/t^{2(k-N)}$

since they contain more than $k - N$ time independent columns of the form $\xi_i^{0,k}$, $i = 1, 2, \dots, N$. Thus S'_k and consequently GALI_k tend to zero following a power law of the form:

$$\text{GALI}_k(t) \propto \frac{1}{t^{2(k-N)}} \text{ for } N < k \leq 2N. \quad (76)$$

4.2.2 The case of $m > 0$ tangent initial deviation vectors

Finally, let us consider the behavior of GALI_k for the special case where m initial deviation vectors, with $m \leq k$ and $m \leq N$, are located in the tangent space of the torus. In this case, matrix \mathbf{D} , whose elements appear in the definition of S'_k , has the form given by (65). Thus, all determinants appearing in the definition of S'_k have as a common factor the quantity $1/\prod_{i=1}^{k-m} M_{m+i}(t)$, which decreases to zero following a power law

$$\frac{1}{\prod_{i=1}^{k-m} M_{m+i}(t)} \propto \frac{1}{t^{k-m}}. \quad (77)$$

Proceeding in exactly the same manner as in the $m = 0$ case above, we deduce that, in the case of $2 \leq k \leq N$ the fastest growing $k \times k$ determinants resulting from the matrix $\mathbf{D}^{m,k}$ are of the form:

$$\left| \eta_{i_1}^k \eta_{i_2}^k \cdots \eta_{i_m}^k \omega_{i_{m+1}n_1} \xi_{n_1}^{0,k} t \omega_{i_{m+2}n_2} \xi_{n_2}^{0,k} t \cdots \omega_{i_k n_{k-m}} \xi_{n_{k-m}}^{0,k} t \right| \propto t^{k-m}, \quad (78)$$

with $i_l \in \{1, 2, \dots, N\}$, $l = 1, 2, \dots, k$ with $i_l \neq i_j$ for $l \neq j$, and $n_l \in \{1, 2, \dots, N\}$, $l = 1, 2, \dots, k - m$ with $n_l \neq n_j$, for $l \neq j$. Hence, we conclude that the behavior of S'_k , and consequently of GALI_k is defined by the behavior of determinants having the form of (78) which, when combined with (77) implies that

$$\text{GALI}_k(t) \approx \text{constant for } 2 \leq k \leq N. \quad (79)$$

The case of $N < k \leq 2N$ deviation vectors, however, with $m > 0$ initially tangent vectors, yields a considerably different result. Following entirely analogous arguments as in the $m = 0$ case, we find that, if $m < k - N$, S'_k and GALI_k evolve proportionally to $t^{2N-k}/t^{k-m} = 1/t^{2(k-N)-m}$. On the other hand, if $m \geq k - N$, one can show that the fastest growing determinant is proportional to t^{N-m} . In this case, S'_k and GALI_k evolve in time following a quite different power law: $t^{N-m}/t^{k-m} = 1/t^{k-N}$.

Summarizing the results of this section, we see that GALI_k for regular motion remains essentially constant when $k \leq N$, while it tends to zero for $k > N$

following a power law which depends on the number m ($m \leq N$ and $m \leq k$) of deviation vectors initially tangent to the torus. In conclusion, we have shown that:

$$\text{GALI}_k(t) \propto \begin{cases} \text{constant} & \text{if } 2 \leq k \leq N \\ \frac{1}{t^{2(k-N)-m}} & \text{if } N < k \leq 2N \text{ and } 0 \leq m < k - N \\ \frac{1}{t^{k-N}} & \text{if } N < k \leq 2N \text{ and } m \geq k - N \end{cases} \quad (80)$$

5 Numerical verification and applications

In order to apply the GALI method to Hamiltonian systems and verify the theoretically predicted behavior of the previous sections, we shall use two simple examples with 2 (2D) and 3 (3D) degrees of freedom: the well-known 2D Hénon–Heiles system [48], described by the Hamiltonian

$$H_2 = \frac{1}{2}(p_x^2 + p_y^2) + \frac{1}{2}(x^2 + y^2) + x^2y - \frac{1}{3}y^3, \quad (81)$$

and the 3D Hamiltonian system:

$$H_3 = \sum_{i=1}^3 \frac{\omega_i}{2}(q_i^2 + p_i^2) + q_1^2q_2 + q_1^2q_3, \quad (82)$$

studied in [49,5]. We keep the parameters of the two systems fixed at the energies $H_2 = 0.125$ and $H_3 = 0.09$, with $\omega_1 = 1$, $\omega_2 = \sqrt{2}$ and $\omega_3 = \sqrt{3}$. In order to illustrate the behavior of GALI_k , for different values of k , we shall consider some representative cases of chaotic and regular orbits of the two systems.

Additionally, we shall study the higher-dimensional example of a 15D Hamiltonian, describing a chain of 15 particles with quadratic and quartic nearest neighbor interaction, known as the famous Fermi–Pasta–Ulam (FPU) model [50]

$$H_{15} = \frac{1}{2} \sum_{i=1}^{15} p_i^2 + \sum_{i=1}^{15} \left[\frac{1}{2}(q_{i+1} - q_i)^2 + \frac{1}{4}\beta(q_{i+1} - q_i)^4 \right] \quad (83)$$

where q_i is the displacement of the i th particle from its equilibrium point and p_i is the conjugate momentum. This is a model we have recently analyzed in [39] and we shall use here the same values of the energy $H_{15} = 26.68777$ and $\beta = 1.04$ as in that study.

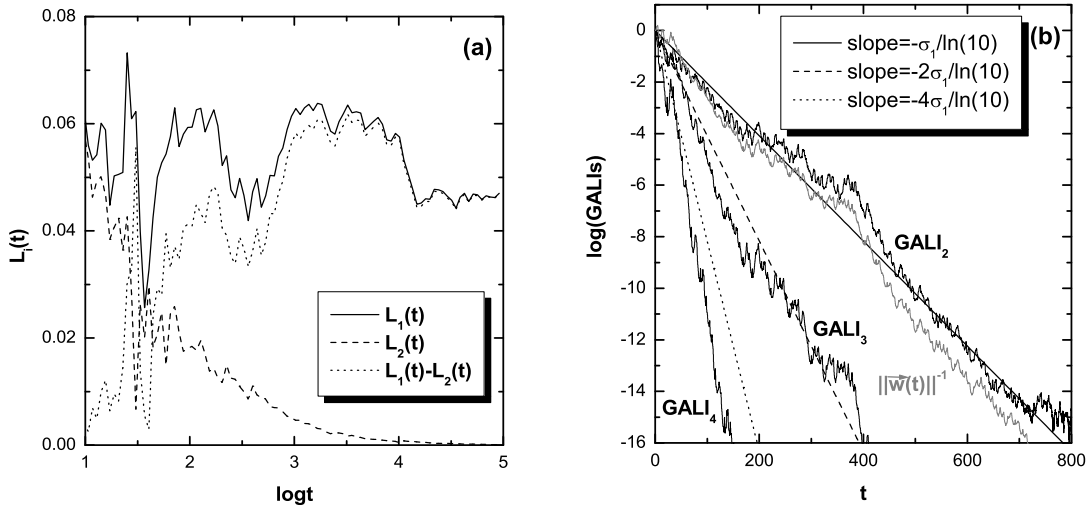


Fig. 1. (a) The evolution of $L_1(t)$ (solid curve), $L_2(t)$ (dashed curve) and $L_1(t) - L_2(t)$ (dotted curve) for a chaotic orbit with initial conditions $x = 0$, $y = -0.25$, $p_x = 0.42$, $p_y = 0$ of the 2D system (81). (b) The evolution of GALI_2 , GALI_3 and GALI_4 of the same orbit. The plotted lines correspond to functions proportional to $e^{-\sigma_1 t}$ (solid line), $e^{-2\sigma_1 t}$ (dashed line) and $e^{-4\sigma_1 t}$ (dotted line) for $\sigma_1 = 0.047$. Note that the t -axis is linear. The evolution of the norm of the deviation vector $\vec{w}(t)$ (with $\|\vec{w}(0)\| = 1$) used for the computation of $L_1(t)$, is also plotted in (b) (gray curve).

5.1 A 2D Hamiltonian system

Let us consider first a chaotic orbit of the 2D Hamiltonian (81), with initial conditions $x = 0$, $y = -0.25$, $p_x = 0.42$, $p_y = 0$. In figure 1(a) we see the time evolution of $L_1(t)$ of this orbit. The computation is carried out until $L_1(t)$ stops having large fluctuations and approaches a positive value (indicating the chaotic nature of the orbit), which could be considered as a good approximation of the maximal LCE, σ_1 . Actually, for $t \approx 10^5$, we find $\sigma_1 \approx 0.047$.

We recall that 2D Hamiltonian systems have only one positive LCE σ_1 , since the second largest is $\sigma_2 = 0$. It also holds that $\sigma_3 = -\sigma_2$ and $\sigma_4 = -\sigma_1$ and thus formula (43), which describes the time evolution of GALI_k for chaotic orbits, gives

$$\text{GALI}_2(t) \propto e^{-\sigma_1 t}, \quad \text{GALI}_3(t) \propto e^{-2\sigma_1 t}, \quad \text{GALI}_4(t) \propto e^{-4\sigma_1 t}. \quad (84)$$

In figure 1(b) we plot GALI_k , $k = 2, 3, 4$ for the same chaotic orbit as a function of time t . We plot t in linear scale so that, if (84) is valid, the slope of GALI_2 , GALI_3 and GALI_4 should approximately be $-\sigma_1/\ln 10$, $-2\sigma_1/\ln 10$

and $-4\sigma_1/\ln 10$ respectively. From figure 1(b) we see that lines having precisely these slopes, for $\sigma_1 = 0.047$, approximate quite accurately the computed values of the GALIs. The biggest deviation between the theoretical curve and numerical data appears in the case of GALI_4 where the theoretical prediction underestimates the decaying rate of the index, but even in this case the difference does not appear too significant. Note, however, the important difference in the times it takes to decide about the chaotic nature of the orbit: Waiting for the maximal LCE to converge in figure 1(a), one needs more than 10^4 time units, while, as we see in figure 1(b), the GALI_k 's provide this information in less than 400 time units!

We also note that, plotting in this example the evolution of the quantity $\|\vec{w}(t)\|^{-1}$ (with $\|\vec{w}(0)\| = 1$), which is used to determine $L_1(t)$ in (1) and is practically identified with the Fast Lyapunov Indicator (FLI), we obtain in figure 1(b) a graph similar to that of $\text{GALI}_2(t)$. This is not surprising, as both $\|\vec{w}(t)\|^{-1}$ and $\text{GALI}_2(t)$ tend exponentially to zero following a decay proportional to $e^{-\sigma_1 t}$ (see equations (30) and (84)). From the results of figure 1(b) we see that the different plotted quantities reach the limit of computer's accuracy (10^{-16}) at different times and in particular GALI_2 at $t \approx 800$, GALI_3 at $t \approx 400$, GALI_4 at $t \approx 150$ and $\|\vec{w}(t)\|^{-1}$ at $t \approx 720$. The CPU time needed for computing the evolution of the indices up to these times were: 0.220 sec for $\|\vec{w}(t)\|^{-1}$, 0.295 sec for GALI_2 , 0.165 sec for GALI_3 and 0.070 sec for GALI_4 respectively. Thus, in this case also, it is clear that the higher order GALI_k (with $k > 2$) can identify the chaotic nature of an orbit faster than the methods of the maximal LCE, the FLI or the SALI (equivalent to GALI_2 , see below).

It is interesting to remark at this point (as mentioned in section 4.1), that the accuracy of the exponential laws (84) is due to the fact that the local Lyapunov exponents cease to fluctuate significantly about their limit values, after a relatively short time interval. To see this, we have plotted in figure 1(a), the two nonnegative local Lyapunov exponents $L_1(t)$, $L_2(t)$, as well as their difference. Note that $L_1(t) - L_2(t)$ begins to be well approximated by $\sigma_1 - \sigma_2 = \sigma_1$ already for times t of order 10^2 units. A similar behavior of such $L_1(t) - L_i(t)$, $i = 2, 3, \dots, 2N$ differences are observed for the other Hamiltonians we studied in this paper having 3 or more degrees of freedom.

As explained in detail in Appendix B, GALI_2 practically coincides with SALI in the case of chaotic orbits. This becomes evident from figure 2 where we plot the absolute difference between GALI_2 and SALI of the chaotic orbit of figure 1 as a function of time t . The two indices practically coincide after about $t \approx 300$ units, since their difference is at the limit of computer's accuracy (10^{-16}), although their actual values are of order 10^{-5} (see figure 1(b)).

Let us now study the behavior of GALI_k for a regular orbit of the 2D Hamil-

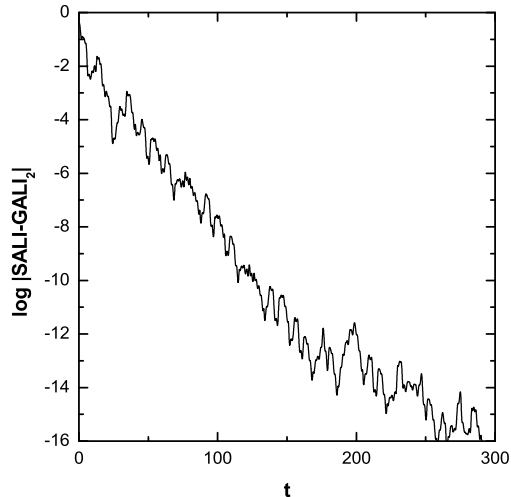


Fig. 2. The absolute difference between GALI_2 and SALI of the chaotic orbit of figure 1 as a function of time t .

tonian (81). From (80) it follows that in the case of a Hamiltonian system with $N = 2$ degrees of freedom GALI_2 will always remain different from zero, while GALI_3 and GALI_4 should decay to zero following a power law, whose exponent depends on the number m of deviation vectors that are initially tangent to the torus on which the orbit lies. Now, for a regular orbit of the 2D Hamiltonian (81) and a random choice of initial deviation vectors, we expect the GALI indices to behave as

$$\text{GALI}_2(t) \propto \text{constant}, \quad \text{GALI}_3(t) \propto \frac{1}{t^2}, \quad \text{GALI}_4(t) \propto \frac{1}{t^4}. \quad (85)$$

A simple qualitative way of studying the dynamics of a Hamiltonian system is by plotting the successive intersections of the orbits with a Poincaré Surface of Section (PSS) [45]. In 2D Hamiltonians, the PSS is a two dimensional plane and the points of a regular orbit (which lie on a torus) fall on a smooth closed curve. This property allows us to choose initial deviation vectors tangent to a torus in the case of system (81). In particular, we consider the regular orbit with initial conditions $x = 0$, $y = 0$, $p_x = 0.5$, $p_y = 0$. In figure 3, we plot the intersection points of this orbit with the PSS defined by $x = 0$ (panel (a)) and $y = 0$ (panel (b)). From the morphology of the two closed curves of figure 3, it is easily seen that deviation vectors $\hat{e}_1 = (1, 0, 0, 0)$ and $\hat{e}_4 = (0, 0, 0, 1)$ are tangent to the torus.

In Figure 4, we plot the time evolution of SALI , GALI_2 , GALI_3 and GALI_4 for the regular orbit of figure 3, for various choices of initial deviation vectors.

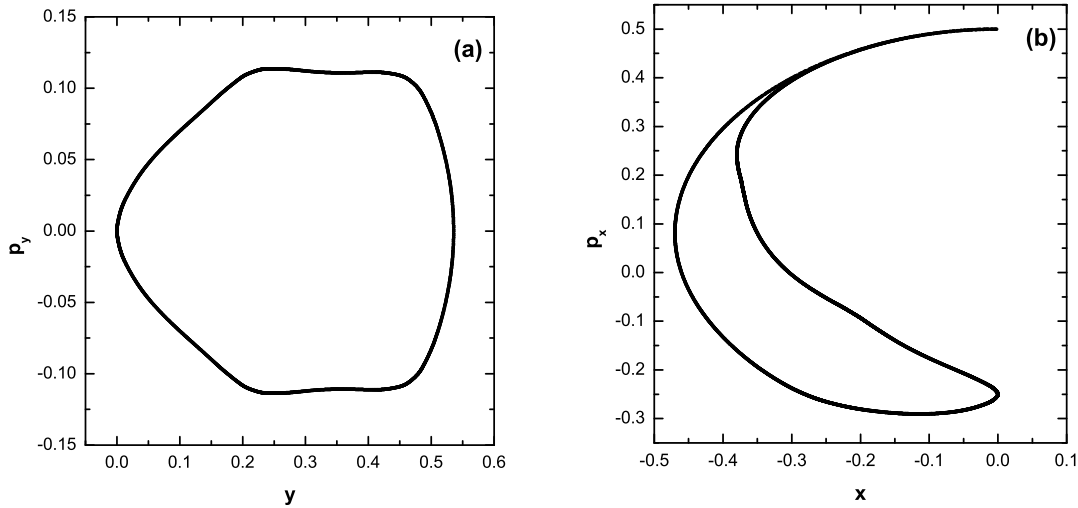


Fig. 3. The Poincaré Surface of Section (PSS) defined by (a) $x = 0$ and (b) $y = 0$ of the regular orbit with initial conditions $x = 0$, $y = 0$, $p_x = 0.5$, $p_y = 0$ for the Hénon–Heiles system (81).

In figure 4(a) the initial deviation vectors are randomly chosen so that none of them is tangent to the torus. In this case SALI and GALI_2 fluctuate around non-zero values, while GALI_3 and GALI_4 tend to zero following the theoretically predicted power laws, see (85). In figure 4(b) we present results for the indices when we have $m = 1$ initial deviation vector tangent to the torus (in particular vector \hat{e}_1). In this case the indices evolve as predicted by (80), i. e. SALI and GALI_2 remain practically constant, while $\text{GALI}_3 \propto 1/t$ and $\text{GALI}_4 \propto 1/t^3$. Finally, in figure 4(c) we have plotted our results using $m = 2$ initial deviation vectors tangent to the torus (vectors \hat{e}_1 and \hat{e}_4). Again the predictions of (80) are seen to be valid since $\text{GALI}_3 \propto 1/t$ and $\text{GALI}_4 \propto 1/t^2$.

The different behavior of SALI (or GALI_2) for regular and chaotic orbits has already been successfully used for discriminating between regions of order and chaos in various dynamical systems [17,36,40,41,42,43,44]. For example, by integrating orbits whose initial conditions lie on a grid, and by attributing to each grid point a color according to the value of SALI at the end of a given integration time, one can obtain clear and informative pictures of the dynamics in the full phase space of several Hamiltonian systems of physical significance [17,36,43].

Figures 1(b) and 4 clearly illustrate that GALI_3 and GALI_4 tend to zero both for regular and chaotic orbits, but with very different time rates. We may use this difference to distinguish between chaotic and regular motion following a different approach than SALI or GALI_2 . Let us illustrate this by considering

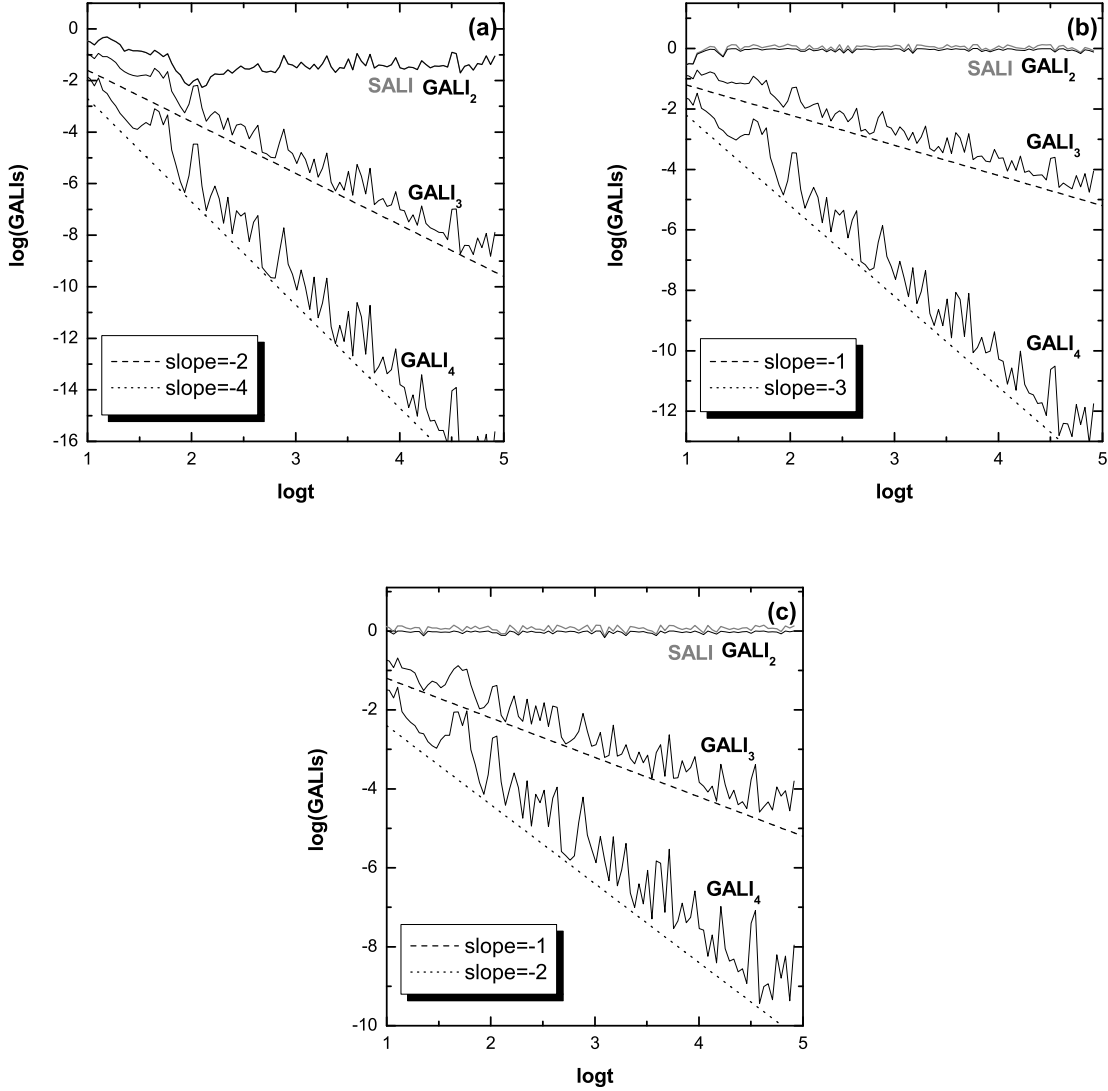


Fig. 4. Time evolution of SALI (gray curves), $GALI_2$, $GALI_3$ and $GALI_4$ for the regular orbit of figure 3 in log–log scale for different values of the number m of deviation vectors initially tangent to the torus: (a) $m = 0$, (b) $m = 1$ and (c) $m = 2$. We note that in panel (a) the curves of SALI and $GALI_2$ are very close to each other and thus cannot be distinguished. In every panel, dashed lines corresponding to particular power laws are also plotted.

the computation of $GALI_4$: From (84) and (85), we expect $GALI_4 \propto e^{-4\sigma_1 t}$ for chaotic orbits and $GALI_4 \propto 1/t^4$ for regular ones. These time rates imply that, in general, the time needed for the index to become zero is much larger for regular orbits. Thus, instead of simply registering the value of the index at the end of a given time interval (as we do with SALI or $GALI_2$), let us record the time, t_{th} , needed for $GALI_4$ to reach a very small threshold, e. g. 10^{-12} , and color each grid point according to the value of t_{th} .

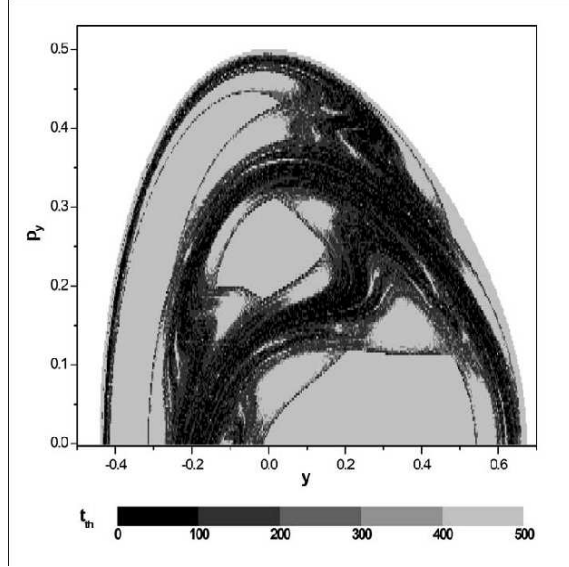


Fig. 5. Regions of different values of the time t_{th} needed for $GALI_4$ to become less than 10^{-12} on the PSS defined by $x = 0$ of the 2D Hénon–Heiles Hamiltonian (81).

The outcome of this procedure for the 2D Hénon–Heiles system (81) is presented in figure 5. Each orbit is integrated up to $t = 500$ units and if the value of $GALI_4$, at the end of the integration is larger than 10^{-12} the corresponding grid point is colored by the light gray color used for $t_{th} \geq 400$. Thus we can clearly distinguish in this figure among various ‘degrees’ of chaotic behavior in regions colored black or dark gray – corresponding to small values of t_{th} – and regions of regular motion colored light gray, corresponding to large values of t_{th} . At the border between them we find points having intermediate values of t_{th} which belong to the so-called ‘sticky’ chaotic regions. Thus, this approach yields a very detailed chart of the dynamics, where even tiny islands of stability can be identified inside the large chaotic sea. We note that for every initial condition the same set of initial deviation vectors was used, ensuring the same initial value of $GALI_4$ for all orbits and justifying the dynamical interpretation of the color scale of figure 5.

5.2 A 3D Hamiltonian system

Let us now study the behavior of the GALIs in the case of the 3D Hamiltonian (82). Following [49,5] the initial conditions of the orbits of this system are defined by assigning arbitrary values to the positions q_1, q_2, q_3 , as well as the so-called ‘harmonic energies’ E_1, E_2, E_3 related to the momenta through

$$p_i = \sqrt{\frac{2E_i}{\omega_i}}, \quad i = 1, 2, 3. \quad (86)$$

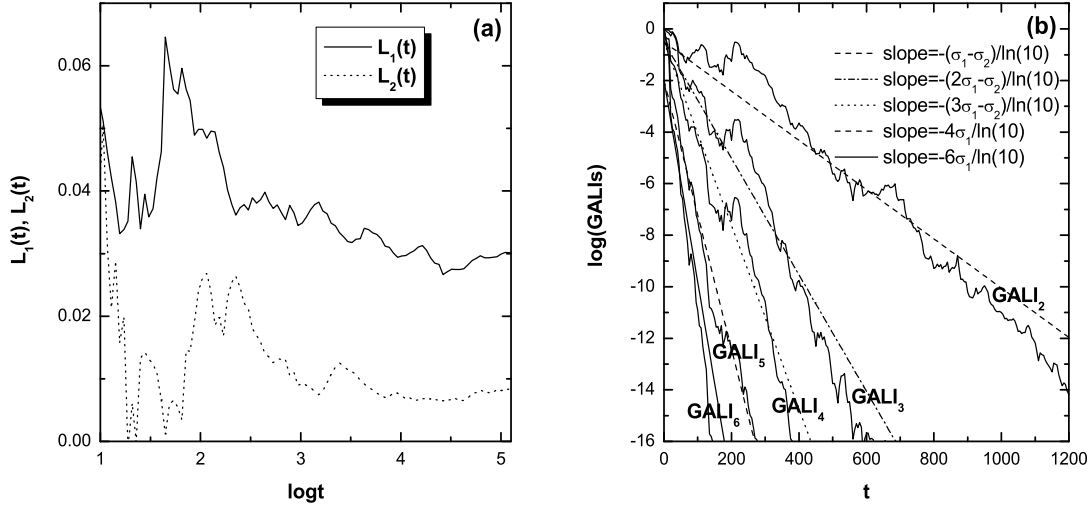


Fig. 6. (a) The evolution of $L_1(t)$, $L_2(t)$ for the chaotic orbit with initial condition $q_1 = q_2 = q_3 = 0$, $E_1 = E_2 = E_3 = 0.03$ of the 3D system (82). (b) The evolution of GALI_k with $k = 2, \dots, 6$ of the same orbit. The plotted lines correspond to functions proportional to $e^{-(\sigma_1 - \sigma_2)t}$, $e^{-(2\sigma_1 - \sigma_2)t}$, $e^{-(3\sigma_1 - \sigma_2)t}$, $e^{-4\sigma_1 t}$ and $e^{-6\sigma_1 t}$ for $\sigma_1 = 0.03$, $\sigma_2 = 0.008$. Note that the t -axis is linear.

Chaotic orbits of 3D Hamiltonian systems generally have two positive Lyapunov exponents, σ_1 and σ_2 , while $\sigma_3 = 0$. So, for approximating the behavior of GALIs according to (43), both σ_1 and σ_2 are needed. In particular, (43) gives

$$\begin{aligned} \text{GALI}_2(t) \propto e^{-(\sigma_1 - \sigma_2)t}, \quad \text{GALI}_3(t) \propto e^{-(2\sigma_1 - \sigma_2)t}, \quad \text{GALI}_4(t) \propto e^{-(3\sigma_1 - \sigma_2)t}, \\ \text{GALI}_5(t) \propto e^{-4\sigma_1 t}, \quad \text{GALI}_6(t) \propto e^{-6\sigma_1 t}. \end{aligned} \quad (87)$$

Let us consider the chaotic orbit with initial conditions $q_1 = q_2 = q_3 = 0$, $E_1 = E_2 = E_3 = 0.03$ of the 3D system (82). We compute σ_1 , σ_2 for this orbit as the long time limits of the Lyapunov exponent quantities $L_1(t)$, $L_2(t)$, applying the technique proposed by Benettin et al. [5]. The results are presented in figure 6(a). The computation is carried out until $L_1(t)$ and $L_2(t)$ stop having large fluctuations and approach some positive values (since the orbit is chaotic), which could be considered as good approximations of their limits σ_1 , σ_2 . Actually for $t \approx 10^5$ we have $\sigma_1 \approx 0.03$ and $\sigma_2 \approx 0.008$. Using these values as good approximations of σ_1 , σ_2 we see in figure 6(b) that the slopes of all GALIs are well reproduced by (87).

Next, we consider the case of regular orbits in our 3D Hamiltonian system. In the general case, where no initial deviation vector is tangent to the torus

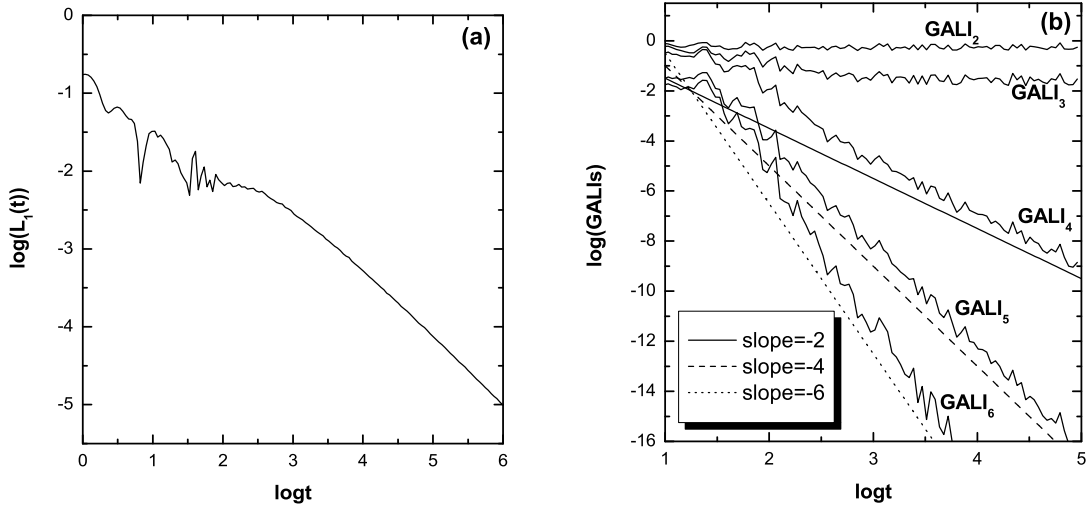


Fig. 7. (a) The evolution of $L_1(t)$ for the regular orbit with initial condition $q_1 = q_2 = q_3 = 0$, $E_1 = 0.005$, $E_2 = 0.085$, $E_3 = 0$ of the 3D system (82). (b) The evolution of GALI_k with $k = 2, \dots, 6$ of the same orbit. The plotted lines correspond to functions proportional to $\frac{1}{t^2}$, $\frac{1}{t^4}$ and $\frac{1}{t^6}$.

where the regular orbit lies, the GALIs should behave as:

$$\begin{aligned} \text{GALI}_2(t) \propto \text{constant}, \quad \text{GALI}_3(t) \propto \text{constant}, \quad \text{GALI}_4(t) \propto \frac{1}{t^2}, \\ \text{GALI}_5(t) \propto \frac{1}{t^4}, \quad \text{GALI}_6(t) \propto \frac{1}{t^6}. \end{aligned} \quad (88)$$

according to (80). In order to verify expression (88) we shall follow a specific regular orbit of the 3D system (82) with initial conditions $q_1 = q_2 = q_3 = 0$, $E_1 = 0.005$, $E_2 = 0.085$, $E_3 = 0$. The regular nature of the orbit is revealed by the slow convergence of its $L_1(t)$ to zero, implying that $\sigma_1 = 0$, see figure 7(a). In figure 7(b), we plot the values of all GALIs of this orbit with respect to time t . From these results we see that the different behaviors of GALIs are very well approximated by formula (88).

From the results of figures 6 and 7, therefore, we conclude that in the case of 3D Hamiltonian systems not only GALI_2 , but also GALI_3 has different behavior for regular and chaotic orbits. In particular GALI_3 tends exponentially to zero for chaotic orbits (even faster than GALI_2 or SALI), while it fluctuates around non-zero values for regular orbits. Hence, the natural question arises whether GALI_3 can be used instead of SALI for the faster detection of chaotic and regular motion in 3D Hamiltonians and, by extension, whether GALI_k , with $k > 3$, should be preferred for systems with $N > 3$. The obvious computational drawback, of course, is that the evaluation of GALI_k requires that we numerically follow the evolution of more than 2 deviation vectors.

First of all, let us point out that the computation of SALI, applying (6), is slightly faster than GALI_2 , for which one needs to evaluate several 2×2 determinants. For example, for orbits of the 3D Hamiltonian (82) the CPU time needed for the computation of SALI for a fixed time interval t , was about 97% of the CPU time needed for the computation of GALI_2 for the same time interval. Although this difference is not significant, we prefer to compute SALI instead of GALI_2 and compare its efficiency with the computation of GALI_3 .

It is obvious that the computation of GALI_3 for a given time interval t needs more CPU time than SALI, since we follow the evolution of three deviation vectors instead of two. This is particularly true for regular orbits as the index does not become zero and its evolution has to be followed for the whole prescribed time interval. In the case of chaotic orbits, however, the situation is different. Let us consider, for example, the chaotic orbit of figure 6. The usual technique to characterize an orbit as chaotic is to check, after some time interval, if its SALI has become less than a very small threshold value, e. g. 10^{-8} . For this particular orbit, this threshold value was reached for $t \approx 760$. Adopting the same threshold to characterize an orbit as chaotic, we find that GALI_3 becomes less than 10^{-8} after $t \approx 335$, requiring only as much as 65% of the CPU time needed for SALI to reach the same threshold!

So, using GALI_3 instead of SALI, we gain considerably in CPU time for chaotic orbits, while we lose for regular orbits. Thus, the efficiency of using GALI_3 for discriminating between chaos and order in a 3D system depends on the percentage of phase space occupied by chaotic orbits (if all orbits are regular GALI_3 requires more CPU time than SALI). More crucially, however, it depends on the choice of the final time, up to which each orbit is integrated. As an example, let us integrate, up to $t = 1000$ time units, all orbits whose initial conditions lie on a dense grid in the subspace $q_3 = p_3 = 0$, $p_2 \geq 0$ of a 4-dimensional PSS, with $q_1 = 0$ of the 3D system (82), attributing to each grid point a color according to the value of GALI_3 at the end of the integration. If GALI_3 of an orbit becomes less than 10^{-8} for $t < 1000$ the evolution of the orbit is stopped, its GALI_3 value is registered and the orbit is characterized as chaotic. The outcome of this experiment is presented in figure 8.

We find that 77% of the orbits of figure 8 are characterized as chaotic, having $\text{GALI}_3 < 10^{-8}$. In order to have the same percentage of orbits identified as chaotic using SALI (i. e. having $\text{SALI} < 10^{-8}$) the same experiment has to be carried out for $t = 2000$ units, requiring 53% more CPU time. Due to the high percentage of chaotic orbits, in this case, even when the SALI is computed for $t = 1000$ the corresponding CPU time is 12% higher than the one needed for the computation of figure 8, while only 55% of the orbits are identified as chaotic. Thus it becomes evident that a carefully designed application of GALI_3 – or GALI_k for that matter – can significantly diminish the computational time needed for a reliable discrimination between regions

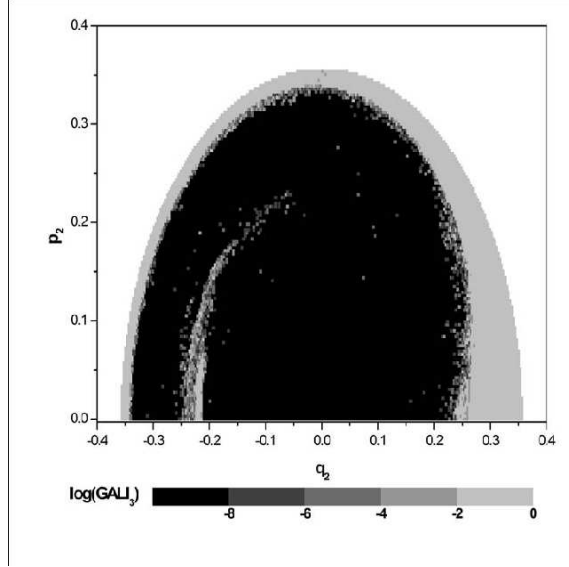


Fig. 8. Regions of different values of the GALI_3 on the subspace $q_3 = p_3 = 0$, $p_2 \geq 0$ of the 4-dimensional PSS $q_1 = 0$ of the 3D system (82) at $t = 1000$.

of order and chaos in Hamiltonian systems with $N > 2$ degrees of freedom.

5.3 A multi-dimensional Hamiltonian system

Let us finally turn to a much higher-dimensional Hamiltonian system having 15 degrees of freedom, i. e. the one shown in (83). With fixed boundary conditions

$$q_0(t) = q_{16}(t) = 0, \quad \forall t, \quad (89)$$

it is known that there exists, for all energies, $H_{15} = E$, a simple periodic orbit, satisfying [51,39]

$$q_{2i}(t) = 0, \quad q_{2i-1}(t) = -q_{2i+1}(t) = q(t), \quad i = 1, 2, \dots, 7, \quad (90)$$

where $q(t) = q(t + T)$ obeys a simple nonlinear equation admitting Jacobi elliptic function solutions. For the parameter values $H_{15} = 26.68777$ and $\beta = 1.04$ used in an earlier study [39], we know that this orbit is unstable and has a sizable chaotic region around it. As initial conditions for (90) we take

$$q(0) = 1.322 \quad \text{and} \quad p_i(0) = 0, \quad i = 1, 2, \dots, 15. \quad (91)$$

First, we consider a chaotic orbit which is located close to this periodic solution, by taking as initial conditions $q_1(0) = q(0)$, $q_3(0) = q_7(0) = q_{11}(0) =$

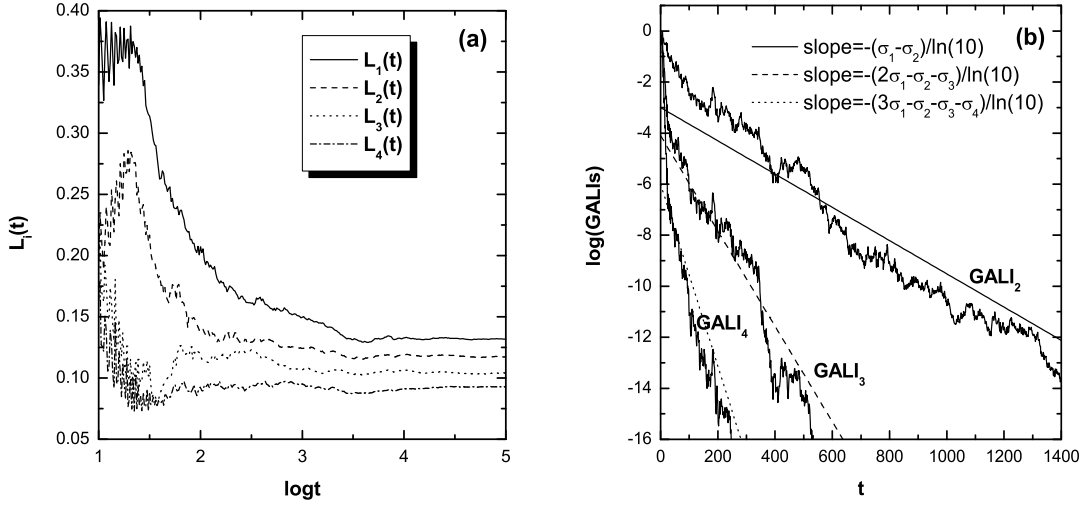


Fig. 9. (a) The evolution of $L_1(t)$, $L_2(t)$, $L_3(t)$ and $L_4(t)$ for a chaotic orbit of the 15D system (83). (b) The evolution of $GALI_2$, $GALI_3$ and $GALI_4$ for the same orbit. The plotted lines correspond to functions proportional to $e^{-(\sigma_1-\sigma_2)t}$, $e^{-(2\sigma_1-\sigma_2-\sigma_3)t}$ and $e^{-(3\sigma_1-\sigma_2-\sigma_3-\sigma_4)t}$, for $\sigma_1 = 0.132$, $\sigma_2 = 0.117$, $\sigma_3 = 0.104$, $\sigma_4 = 0.093$. Note that the t -axis is linear.

$-q(0) + 10^{-7}$, $q_5(0) = q_9(0) = q_{15}(0) = q(0) - 10^{-7}$, $q_{2i} = 0$ for $i = 1, 2, \dots, 7$ and $p_i(0) = 0$ for $i = 1, 2, \dots, 14$, $p_{15}(0) = 0.00323$. The chaotic nature of this orbit is revealed by the fact that its maximal LCE is positive (see figure 9(a)). In fact, from the results of figure 9(a) we deduce reliable estimates of the system's four largest Lyapunov exponents: $\sigma_1 \approx 0.132$, $\sigma_2 \approx 0.117$, $\sigma_3 \approx 0.104$ and $\sigma_4 \approx 0.093$. Thus, we have a case where several LCEs have positive values, the largest two of them being very close to each other. The behavior of the GALIs is again quite accurately approximated by the theoretically predicted exponential laws (43). This becomes evident by the results presented in figure 9(b), where we plot the time evolution of $GALI_2$, $GALI_3$ and $GALI_4$ as well as the exponential laws that theoretically describe the evolution of these indices. In this case, $GALI_2$ does decay to zero relatively slowly since σ_1 and σ_2 have similar values and hence, using $GALI_3$, $GALI_4$ or a GALI of higher order, one can determine the chaotic nature of the orbit much faster.

It is worth mentioning that (43) describes much more accurately the evolution of $GALI_k$ when the orbit we wish to study is very close to the unstable periodic solution (90) itself. This is due to the fact that in that case, the LCEs are directly related to the eigenvalues of the monodromy matrix associated with the variational equations of this unstable periodic orbit, see equation (25). In fact, for our choice of parameters, this matrix has two equal pairs of real eigenvalues with magnitude greater than one, while all other eigenvalues lie on the unit circle in the complex plane. As a consequence, the orbit has two nearly identical positive Lyapunov exponents (as well as their two negative

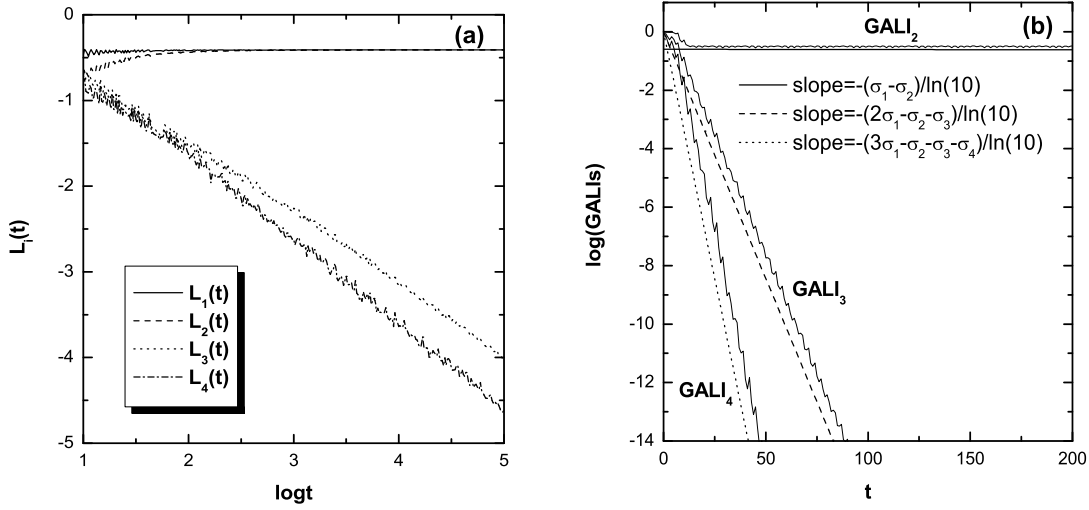


Fig. 10. (a) The evolution of $L_1(t)$, $L_2(t)$, $L_3(t)$ and $L_4(t)$ for an orbit which is very close to the unstable periodic orbit (91) of the 15D system (83). (b) The evolution of GALI_2 , GALI_3 and GALI_4 of the same orbit. The plotted lines correspond to functions proportional to $e^{-(\sigma_1 - \sigma_2)t}$, $e^{-(2\sigma_1 - \sigma_2 - \sigma_3)t}$ and $e^{-(3\sigma_1 - \sigma_2 - \sigma_3 - \sigma_4)t}$, for $\sigma_1 = 0.3885$, $\sigma_2 = 0.3883$, $\sigma_3 = 0$, $\sigma_4 = 0$. Note that the t -axis is linear.

counterparts), while all other exponents are zero. This is shown in figure 10(a), where we plot the evolution of the $L_i(t)$ for $i = 1, 2, 3, 4$, whose limits for $t \rightarrow \infty$ are the 4 largest Lyapunov exponents. From these results we deduce $\sigma_1 \approx 0.3885$, $\sigma_2 \approx 0.3883$, while the decrease of $L_3(t)$ and $L_4(t)$ to zero indicate that $\sigma_3 = \sigma_4 = 0$. In figure 10(b) we now observe that GALI_2 remains practically constant for this particular time interval (actually it decreases to zero extremely slowly following the exponential law $e^{-(\sigma_1 - \sigma_2)t} = e^{-0.0002t}$). On the other hand, GALI_3 and GALI_4 decay exponentially to zero following the laws, $\text{GALI}_3 \propto e^{-(2\sigma_1 - \sigma_2 - \sigma_3)t}$, $\text{GALI}_4 \propto e^{-(3\sigma_1 - \sigma_2 - \sigma_3 - \sigma_4)t}$, given by equation (43).

6 Discussion and conclusions

In this paper we have introduced and applied the Generalized Alignment Indices of order k (GALI_k) as a tool for studying local and global dynamics in conservative dynamical systems, such as Hamiltonian systems of N degrees of freedom, or $2N$ -dimensional symplectic maps. We have shown that these indices can be successfully employed not only to distinguish individual orbits as chaotic or regular, but also to efficiently chart large domains of phase space, characterizing the dynamics in the various regions by different behaviors of the indices ranging from regular (GALI_k s are constant or decay by well-defined power laws) to chaotic (GALI_k s exponentially go to zero).

A different approach than simply calculating the maximal Lyapunov exponent is to compute the so-called Smaller Alignment Index (SALI), following the evolution of *two* initially different deviation vectors. This approach has been used by several authors and has proved quite successful, as it can determine the nature of the dynamics more rapidly, reliably and efficiently than the maximal LCE. In the present paper, motivated by the observation that the SALI is in fact proportional to the ‘area’ of a parallelogram, having as edges the two normalized deviation vectors, we have generalized SALI by defining a quantity called GALI_k , representing the ‘volume’ of a parallelepiped having as edges $k > 2$ initially linearly independent unit deviation vectors. In practice, GALI_k is computed as the ‘norm’ of the ‘exterior’ or wedge product of the k normalized deviation vectors.

For the numerical evaluation of GALI_k , we need to compute the reference orbit we are interested in from the fully nonlinear equations of the system, as well as follow the time evolution of k deviation vectors, solving the (linear) variational equations about the orbit. How many such vectors should we take? Since the phase space of the dynamical system is $2N$ -dimensional, k should be less than or equal to $2N$, otherwise GALI_k will be equal to zero already from the start. However, even though we may choose our deviation vectors initially linearly independent, they may *become dependent* as time evolves, in which case the phase space ‘volume’ represented by GALI_k will vanish! This is precisely what happens for all $k > 2$ if our reference orbit is chaotic, and also if it is regular and $k > N$, but at very different time rates.

In particular, we showed analytically and verified numerically in a number of examples of Hamiltonian systems that for chaotic orbits GALI_k tends exponentially to zero following a rate which depends on the values of several Lyapunov exponents (see equation (43)). On the other hand, in the case of regular orbits, GALI_k with $2 \leq k \leq N$ fluctuates around non-zero values, while, for $N < k \leq 2N$, it tends to zero following a power law (see equation (80)). The exponent of the power law depends on the values of k and N , as well as on the number m of deviation vectors that may have been chosen initially tangent to the torus on which the orbit lies.

Clearly, these different behaviors of the GALI_k can be exploited for the rapid and accurate determination of the chaotic versus regular nature of a given orbit, or of an ensemble of orbits. Varying the number of deviation vectors (and bringing more LCEs into play), we can, in fact, achieve high rates of identification of chaotic regions, in a computationally advantageous way. Secondly, regular motion can be identified by the index being nearly constant for small k , while, when k exceeds the dimension of the orbits’ subspace, GALI_k decays by well-defined power laws. This may help us identify, for example, cases where the motion occurs on cantori of dimension $d < N$ (see e.g. [45]) and the orbits become ‘sticky’ on island chains, before turning truly chaotic

and exponential decay takes over.

We have also studied on specific Hamiltonians with $N > 2$ the *computational efficiency* of the GALI_k . One might suspect, of course, that the best choice would be GALI_N since this is the index that exhibits the most different behavior for regular and chaotic orbits. On the other hand, it is clear that following a great number of deviation vectors requires considerably more computation time. It turns out, however, that, if chaos occupies a ‘large’ portion of phase space, a well-tailored application of GALI_k , with $2 < k \leq N$, can significantly diminish the CPU time required for the detailed ‘charting’ of phase space, compared with SALI ($k = 2$), as we demonstrated on specific examples in section 5.2 (see figure 8).

Although the results presented in this paper were obtained for N degree of freedom Hamiltonian systems, it is easy to see that they also apply to $2N$ -dimensional symplectic maps. So, equations (43) and (80) which describe the behavior of GALI_k , with $2 \leq k \leq 2N$, for chaotic and regular orbits respectively are expected to hold in that case also. One remark is in order, however: In the case of $N = 1$, i. e. for 2D maps, the first condition of equation (80) cannot be fulfilled. Thus, for regular orbits of 2D maps, any 2 initially independent deviation vectors will become aligned in the direction tangent to the corresponding invariant curve and GALI_2 will tend to zero following a power law of the form $\text{GALI}_2 \propto 1/t^2$. This behavior is already known in the literature [15].

Acknowledgements

This work was partially supported by the European Social Fund (ESF), Operational Program for Educational and Vocational Training II (EPEAEK II) and particularly the Programs HERAKLEITOS, providing a Ph. D. scholarship for the third author (C. A.) and the Program PYTHAGORAS II, partially supporting the first author (Ch. S.). Ch. S. was also supported by the Marie Curie Intra-European Fellowship No MEIF-CT-2006-025678. The second author (T. B.) wishes to express his gratitude to the beautiful Centro Internacional de Ciencias of the Universidad Autonoma de Mexico for its excellent hospitality during his visit in January – February 2006, when some of this work was completed. In particular, T. B. wants to thank the main researchers of this Center, Dr. Christof Jung and Thomas Seligman for numerous conversations on the stability of multi-dimensional Hamiltonian systems. Finally, we would like to thank the referees for very useful comments which helped us improve the clarity of the paper.

A Wedge product

Following an introduction to the theory of wedge products as presented in textbooks such as [52], let us consider an M -dimensional vector space V over the field of real numbers \mathbb{R} . The exterior algebra of V is denoted by $\Lambda(V)$ and its multiplication, known as the wedge product or the exterior product, is written as \wedge . The wedge product is associative:

$$(\vec{u} \wedge \vec{v}) \wedge \vec{w} = \vec{u} \wedge (\vec{v} \wedge \vec{w}) \quad (\text{A.1})$$

for $\vec{u}, \vec{v}, \vec{w} \in V$ and bilinear

$$\begin{aligned} (c_1 \vec{u} + c_2 \vec{v}) \wedge \vec{w} &= c_1(\vec{u} \wedge \vec{w}) + c_2(\vec{v} \wedge \vec{w}), \\ \vec{w} \wedge (c_1 \vec{u} + c_2 \vec{v}) &= c_1(\vec{w} \wedge \vec{u}) + c_2(\vec{w} \wedge \vec{v}) \end{aligned} \quad (\text{A.2})$$

for $\vec{u}, \vec{v}, \vec{w} \in V$ and $c_1, c_2 \in \mathbb{R}$. The wedge product is also alternating on V

$$\vec{u} \wedge \vec{u} = \vec{0} \quad (\text{A.3})$$

for all vectors $\vec{u} \in V$. Thus we have that

$$\vec{u} \wedge \vec{v} = -\vec{v} \wedge \vec{u} \quad (\text{A.4})$$

for all vectors $\vec{u}, \vec{v} \in V$ and

$$\vec{u}_1 \wedge \vec{u}_2 \wedge \cdots \wedge \vec{u}_k = \vec{0} \quad (\text{A.5})$$

whenever $\vec{u}_1, \vec{u}_2, \dots, \vec{u}_k \in V$ are linearly dependent.

Elements of the form $\vec{u}_1 \wedge \vec{u}_2 \wedge \cdots \wedge \vec{u}_k$ with $\vec{u}_1, \vec{u}_2, \dots, \vec{u}_k \in V$ are called k -vectors. The subspace of $\Lambda(V)$ generated by all k -vectors is called the k -th exterior power of V and denoted by $\Lambda^k(V)$. The exterior algebra $\Lambda(V)$ can be written as the direct sum of each of the k -th powers of V :

$$\Lambda(V) = \bigoplus_{k=0}^M \Lambda^k(V) = \Lambda^0(V) \oplus \Lambda^1(V) \oplus \Lambda^2(V) \oplus \cdots \oplus \Lambda^M(V) \quad (\text{A.6})$$

where $\Lambda^0(V) = \mathbb{R}$ and $\Lambda^1(V) = V$.

Let $\{\hat{e}_1, \hat{e}_2, \dots, \hat{e}_M\}$ be an orthonormal basis of V , i. e. \hat{e}_i , $i = 1, 2, \dots, M$ are linearly independent vectors of unit magnitude and

$$\hat{e}_i \cdot \hat{e}_j = \delta_{ij} \quad (\text{A.7})$$

where (\cdot) denotes the inner product in V and

$$\delta_{ij} = \begin{cases} 1 & \text{for } i = j \\ 0 & \text{for } i \neq j \end{cases}. \quad (\text{A.8})$$

It can be easily seen that the set

$$\{\hat{e}_{i_1} \wedge \hat{e}_{i_2} \wedge \cdots \wedge \hat{e}_{i_k} \mid 1 \leq i_1 < i_2 < \cdots < i_k \leq M\} \quad (\text{A.9})$$

is a basis of $\Lambda^k(V)$ since any wedge product of the form $\vec{u}_1 \wedge \vec{u}_2 \wedge \cdots \wedge \vec{u}_k$ can be written as a linear combination of the k -vectors of equation (A.9). This is true because every vector \vec{u}_i , $i = 1, 2, \dots, k$ can be written as a linear combination of the basis vectors \hat{e}_i , $i = 1, 2, \dots, M$ and using the bilinearity of the wedge product this can be expanded to a linear combination of wedge products of those basis vectors. Any wedge product in which the same basis vector appears more than once is zero, while any wedge product in which the basis vectors do not appear in the proper order can be reordered, changing the sign whenever two basis vectors change places. The dimension of $\Lambda^k(V)$ is equal to the binomial coefficient

$$\dim \Lambda^k(V) = \binom{M}{k} = \frac{M!}{k!(M-k)!} \quad (\text{A.10})$$

and thus the dimension of $\Lambda(V)$ is equal to the sum of the binomial coefficients

$$\dim \Lambda(V) = \sum_{k=0}^M \binom{M}{k} = 2^M. \quad (\text{A.11})$$

The coefficients of a k -vector $\vec{u}_1 \wedge \vec{u}_2 \wedge \cdots \wedge \vec{u}_k$ are the minors of the matrix that describes the vectors \vec{u}_i , $i = 1, 2, \dots, k$ in terms of the basis \hat{e}_i , $i = 1, 2, \dots, M$. Let us write these relations in matrix form

$$\begin{bmatrix} \vec{u}_1 \\ \vec{u}_2 \\ \vdots \\ \vec{u}_k \end{bmatrix} = \begin{bmatrix} u_{11} & u_{12} & \cdots & u_{1M} \\ u_{21} & u_{22} & \cdots & u_{2M} \\ \vdots & \vdots & & \vdots \\ u_{k1} & u_{k2} & \cdots & u_{kM} \end{bmatrix} \cdot \begin{bmatrix} \hat{e}_1 \\ \hat{e}_2 \\ \vdots \\ \hat{e}_M \end{bmatrix} = \mathbf{C} \cdot \begin{bmatrix} \hat{e}_1 \\ \hat{e}_2 \\ \vdots \\ \hat{e}_M \end{bmatrix} \quad (\text{A.12})$$

\mathbf{C} being the matrix of the coefficients of vectors \vec{u}_i , $i = 1, 2, \dots, k$ with respect to the orthonormal basis \hat{e}_i , $i = 1, 2, \dots, M$ and u_{ij} , $i = 1, 2, \dots, k$, $j =$

$1, 2, \dots, M$ being real numbers. Then the wedge product $\vec{u}_1 \wedge \vec{u}_2 \wedge \dots \wedge \vec{u}_k$ is defined by

$$\vec{u}_1 \wedge \vec{u}_2 \wedge \dots \wedge \vec{u}_k = \sum_{1 \leq i_1 < i_2 < \dots < i_k \leq M} \begin{vmatrix} u_{1i_1} & u_{1i_2} & \dots & u_{1i_k} \\ u_{2i_1} & u_{2i_2} & \dots & u_{2i_k} \\ \vdots & \vdots & & \vdots \\ u_{ki_1} & u_{ki_2} & \dots & u_{ki_k} \end{vmatrix} \hat{e}_{i_1} \wedge \hat{e}_{i_2} \wedge \dots \wedge \hat{e}_{i_k} \quad (\text{A.13})$$

where the sum is performed over all possible combinations of k indices out of the M total indices. So the coefficient of a particular k -vector $\hat{e}_{i_1} \wedge \hat{e}_{i_2} \wedge \dots \wedge \hat{e}_{i_k}$ is the determinant of the $k \times k$ submatrix of the $k \times M$ matrix of coefficients appearing in equation (A.12) formed by its i_1, i_2, \dots, i_k columns.

B The relation between GALI₂ and SALI

Proposition 1 *We consider a $2N$ -dimensional vector space over the field of real numbers \mathbb{R} , which has the usual Euclidean norm and is spanned by the orthonormal basis $\{\hat{e}_1, \hat{e}_2, \dots, \hat{e}_{2N}\}$. We also consider two unit vectors \hat{w}_1, \hat{w}_2 in this space so that*

$$\hat{w}_1 = \sum_{i=1}^{2N} w_{1i} \hat{e}_i, \quad \hat{w}_2 = \sum_{i=1}^{2N} w_{2i} \hat{e}_i, \quad (\text{B.1})$$

and

$$\sum_{i=1}^{2N} w_{1i}^2 = 1, \quad \sum_{i=1}^{2N} w_{2i}^2 = 1. \quad (\text{B.2})$$

Let us now define the 2-vector $\hat{w}_1 \wedge \hat{w}_2$ from equation (A.13) and its norm from equation (18). Under these assumptions the following holds:

$$\|\hat{w}_1 \wedge \hat{w}_2\| = \frac{\|\hat{w}_1 - \hat{w}_2\| \cdot \|\hat{w}_1 + \hat{w}_2\|}{2} \quad (\text{B.3})$$

Proof. Expanding the right hand side of equation (B.3) we have:

$$\mathcal{A} = \left(\frac{\|\hat{w}_1 + \hat{w}_2\| \cdot \|\hat{w}_1 - \hat{w}_2\|}{2} \right)^2 = \frac{\sum_{i=1}^{2N} (w_{1i} - w_{2i})^2 \cdot \sum_{i=1}^{2N} (w_{1i} + w_{2i})^2}{4} =$$

$$\begin{aligned}
&= \frac{1}{4} \cdot \left[\left(\sum_{i=1}^{2N} w_{1i}^2 + \sum_{i=1}^{2N} w_{2i}^2 - 2 \sum_{i=1}^{2N} w_{1i} w_{2i} \right) \cdot \left(\sum_{i=1}^{2N} w_{1i}^2 + \sum_{i=1}^{2N} w_{2i}^2 + 2 \sum_{i=1}^{2N} w_{1i} w_{2i} \right) \right] = \\
&= \left(1 - \sum_{i=1}^{2N} w_{1i} w_{2i} \right) \cdot \left(1 + \sum_{i=1}^{2N} w_{1i} w_{2i} \right) = 1 - \left(\sum_{i=1}^{2N} w_{1i} w_{2i} \right)^2 \Rightarrow \\
&\mathcal{A} = 1 - \left(\sum_{i=1}^{2N} w_{1i}^2 w_{2i}^2 + 2 \sum_{i < j} w_{1i} w_{2i} w_{1j} w_{2j} \right), \quad (\text{B.4})
\end{aligned}$$

where we made use of (B.2). On the other hand, using equation (18) we get for the left hand side of equation (B.3):

$$\begin{aligned}
\mathcal{B} &= \|\hat{w}_1 \wedge \hat{w}_2\|^2 = \sum_{i < j} \left| \begin{array}{cc} w_{1i} & w_{1j} \\ w_{2i} & w_{2j} \end{array} \right|^2 = \sum_{i < j} (w_{1i} w_{2j} - w_{1j} w_{2i})^2 \Rightarrow \\
\mathcal{B} &= \sum_{i < j} w_{1i}^2 w_{2j}^2 + \sum_{i < j} w_{1j}^2 w_{2i}^2 - 2 \sum_{i < j} w_{1i} w_{2i} w_{1j} w_{2j}. \quad (\text{B.5})
\end{aligned}$$

The first two sums of equation (B.5) contain all the possible products of the coordinates of the two vectors except the ones corresponding to equal indices, $i = j$. So the quantity \mathcal{B} can be written as follows:

$$\begin{aligned}
\mathcal{B} &= \sum_{i \neq j} w_{1i}^2 w_{2j}^2 - 2 \sum_{i < j} w_{1i} w_{2i} w_{1j} w_{2j} = \\
&= \sum_{i \neq j} w_{1i}^2 w_{2j}^2 + \sum_{i=1}^{2N} w_{1i}^2 w_{2i}^2 - \left(\sum_{i=1}^{2N} w_{1i}^2 w_{2i}^2 + 2 \sum_{i < j} w_{1i} w_{2i} w_{1j} w_{2j} \right). \quad (\text{B.6})
\end{aligned}$$

Now, the first two sums contain all the possible products between the coordinates of the two vectors and so \mathcal{B} takes the form:

$$\begin{aligned}
\mathcal{B} &= \sum_{i=1}^{2N} \sum_{j=1}^{2N} w_{1i}^2 w_{2j}^2 - \left(\sum_{i=1}^{2N} w_{1i}^2 w_{2i}^2 + 2 \sum_{i < j} w_{1i} w_{2i} w_{1j} w_{2j} \right) = \\
&= \sum_{i=1}^{2N} w_{1i}^2 \cdot \sum_{i=1}^{2N} w_{2i}^2 - \left(\sum_{i=1}^{2N} w_{1i}^2 w_{2i}^2 + 2 \sum_{i < j} w_{1i} w_{2i} w_{1j} w_{2j} \right) \Rightarrow \\
\mathcal{B} &= 1 - \left(\sum_{i=1}^{2N} w_{1i}^2 w_{2i}^2 + 2 \sum_{i < j} w_{1i} w_{2i} w_{1j} w_{2j} \right), \quad (\text{B.7})
\end{aligned}$$

where we used again (B.2). Comparing equations (B.4) and (B.7) we see that both sides of equation (B.3) are equal and so the proof of proposition 1 is complete. ■

Using equation (B.3) as well as the definitions of SALI (6) and GALI_2 (19) we conclude that the precise relation between the two indices is

$$\text{GALI}_2 = \text{SALI} \cdot \frac{\max \{ \|\hat{w}_1 + \hat{w}_2\|, \|\hat{w}_1 - \hat{w}_2\| \}}{2}. \quad (\text{B.8})$$

So, the two indices are proportional to each other

$$\text{GALI}_2 \propto \text{SALI}, \quad (\text{B.9})$$

since the quantity $m = \max \{ \|\hat{w}_1 + \hat{w}_2\|, \|\hat{w}_1 - \hat{w}_2\| \}$ lies in the interval $m \in [\sqrt{2}, 2]$. In particular, in the case of chaotic orbits $m \rightarrow 2$ as $\text{SALI} \rightarrow 0$ and eventually GALI_2 also vanishes, while in the case of regular motion m fluctuates around non-zero values in the above interval $[\sqrt{2}, 2)$.

From the above discussion we conclude that SALI is essentially equivalent to GALI_2 . In practice, however, since the computation of GALI_2 according to equation (18) for $k = 2$, requires the evaluation of several 2×2 determinants, it is more convenient to compute SALI in its place, by performing the simpler computation of equation (6).

References

- [1] Oseledec V I 1968 *Trans. Moscow Math. Soc.* **19** 197
- [2] Benettin G, Galgani L and Strelcyn J-M 1976 *Phys. Rev. A* **14** 2338
- [3] Pesin Y B 1977 *Russian Math. Surveys* **32** 55
- [4] Benettin G, Galgani L, Giorgilli A and Strelcyn J-M 1980 *Meccanica* **March** 9
- [5] Benettin G, Galgani L, Giorgilli A and Strelcyn J-M 1980 *Meccanica* **March** 21
- [6] Greene J M and Kim J-S *Physica D* **24** 213
- [7] Bridges T J and Reich S *Physica D* **156** 219
- [8] Froeschlé C, Lega E and Gonczi R 1997 *Celest. Mech. Dyn. Astron.* **67** 41
- [9] Froeschlé C, Gonczi R and Lega E 1997 *Planet. Space Sci.* **45** 881
- [10] Fouchard M, Lega E, Froeschlé Ch and Froeschlé C 2002 *Celest. Mech. Dyn. Astron.* **83** 205
- [11] Guzzo M, Lega E and Froeschlé C 2002 *Physica D* **163** 1
- [12] Barrio R 2005 *Chaos Sol. Fract.* **25** 711

- [13] Cincotta P M and Simó 2000 *Astron. Astroph. Suppl. Ser.* **147** 205
- [14] Cincotta P M, Giordano C M and Simó C 2003 *Physica D* **182** 151
- [15] Skokos Ch 2001 *J. Phys. A* **34** 10029
- [16] Skokos Ch, Antonopoulos Ch, Bountis T C and Vrahatis M N 2003 *Prog. Theor. Phys. Suppl.* **150** 439
- [17] Skokos Ch, Antonopoulos Ch, Bountis T C and Vrahatis M N 2004 *J. Phys. A* **37** 6269
- [18] Sándor Zs, Érdi B, Széll A and Funk B 2004 *Celest. Mech. Dyn. Astron.* **90** 127
- [19] Vozikis Ch L, Varvoglis H and Tsiganis K 2000 *Astron. Astroph.* **359** 386
- [20] Froeschlé C, Froeschlé Ch and Lohinger E 1993 *Celest. Mech. Dyn. Astron.* **56** 307
- [21] Lohinger E, Froeschlé C and Dvorak R 1993 *Celest. Mech. Dyn. Astron.* **56** 315
- [22] Voglis N and Contopoulos G 1994 *J. Phys. A* **27** 4899
- [23] Laskar J 1990 *Icarus* **88** 266
- [24] Laskar J, Froeschlé C and Celletti A 1992 *Physica D* **56** 253
- [25] Laskar J 1993 *Physica D* **67** 257
- [26] Papaphilippou Y and Laskar J 1996 *Astron. Astrophys.* **307** 427
- [27] Papaphilippou Y and Laskar J 1998 *Astron. Astrophys.* **329** 451
- [28] Laskar J 1999 *Hamiltonian systems with three or more degrees of freedom* (ed. Simó C / Plenum Press) p 134
- [29] Voyatzis G and Ichtiaroglou S 1992 *J. Phys. A* **25** 5931
- [30] Kotoulas T and Voyatzis G 2004 *Celest. Mech. Dyn. Astron.* **88** 343
- [31] Gottwald G A and Melbourne I 2004 *Proc. Roy. Soc. London A* **460** 603
- [32] Sideris I V 2005 *Nonlinear Dynamics in Astronomy and Astrophysics* (*Annals of the New York Academy of Science* vol 1045) ed S T Gottesman, J–R Buchler *et al* (New York: The New York Academy of Sciences)
- [33] Howard J E 2005 *Celest. Mech. Dyn. Astron.* **92** 219
- [34] Skokos Ch, Antonopoulos Ch, Bountis T C and Vrahatis M N 2003 *Libration Point Orbits and Applications* eds G Gomez, M W Lo and J J Masdemont (Singapore: World Scientific) p 653
- [35] Széll A 2003 *PhD Thesis* Glasgow Caledonian University
- [36] Széll A, Érdi B, Sándor Zs and Steves B 2004 *MNRAS* **347** 380
- [37] Panagopoulos P, Bountis T C and Skokos Ch 2004 *J. Vib. & Acoust.* **126** 520

- [38] de Assis L P G, Helayel-Neto J A, Haas F and Nogueira A L M A 2005 On the integrability and chaos of an $N = 2$ Maxwell–Chern–Simons–Higgs mechanical model *Preprint* hep-th/0505159
- [39] Antonopoulos Ch, Bountis T C and Skokos Ch 2006 *Int. J. Bif. & Chaos* **16** 1777
- [40] Manos T, Athanassoula E 2005 *Proceedings of Semaine de l' Astrophysique Française Journées de la SF2A* eds F Caloli, T Contini, J M Hameury and L Pagani (EDP-Science Conference Series) p 631
- [41] Manos T, Athanassoula E 2005 Chaos and the dynamical evolution of barred galaxies *Preprint* astro-ph/0510823
- [42] Manos T, Athanassoula E 2006 *Recent Advances in Astronomy and Astrophysics: 7th International Conference of the Hellenic Astronomical Society* ed N Solomos (AIP Conference Proceedings) **848** p 662
- [43] Bountis T C and Skokos Ch 2006 *Nucl. Inst. Meth. Phys. Res. A* **561** 173
- [44] Capuzzo–Dolcetta R, Leccese L, Merritt D and Vicari A 2006 Self-consistent models of cuspy triaxial galaxies with dark matter haloes *Preprint* astro-ph/0611205
- [45] Lieberman M A and Lichtenberg A J 1992 *Regular and Chaotic Dynamics* (Springer Verlag)
- [46] Cvitanović P, Artuso R, Mainieri R, Tanner G and Vattay G 2005 *Chaos: Classical and Quantum*, <http://ChaosBook.org> (Niels Bohr Institute, Copenhagen)
- [47] Verhulst F 1990 *Nonlinear Differential Equations and Dynamical Systems* (Springer Verlag)
- [48] Hénon M and Heiles C 1964 *Astron. J.* **69** 73
- [49] Contopoulos G, Galgani L and Giorgilli A 1978 *Phys. rev. A* **18** 1183
- [50] Fermi E, Pasta J and Ulam S 1955 *Los Alamos Rep* LA–1940
- [51] Ooyama N, Hirooka H and Saitô N 1969 *J. Phys. Soc. Japan* **27** 815
- [52] Spivak M 1999 *Comprehensive Introduction to Differential Geometry*, vol. 1, (Publ. or Per. Inc.)